Frontiers of Physics
https://doi.org/10.1007/s11467-021-1055-z
Front. Phys.
17(1), 13304 (2022)

REVIEW ARTICLE

Narrow-bandgap materials for optoelectronics applications

Xiao-Hui Li[1,#,†], Yi-Xuan Guo[1,#], Yujie Ren[1,#], Jia-Jun Peng[1,#], Ji-Shu Liu[1], Cong Wang[2], Han Zhang[2,‡]

[1] *School of Physics & Information Technology, Shaanxi Normal University, Xi'an 710119, China*
[2] *Shenzhen Key Laboratory of Two-Dimensional Materials and Devices/Shenzhen Engineering Laboratory of Phosphorene and Optoelectronics, Collaborative Innovation Center for Optoelectronic Science and Technology, Key Laboratory of Optoelectronic Devices and Systems of Ministry of Education and Guangdong, Shenzhen 518060, China*
Corresponding authors. E-mail: †lixiaohui@snnu.edu.cn, ‡hzhang@szu.edu.cn
Received October 17, 2020; accepted January 2, 2021

Narrow-bandgap materials possess the intriguing optical–electric properties and unique structures, which can be widely applied in the field of photonics, energy optoelectronic sensing and biomedicine, etc. Nowadays, the researches on nonlinear optical properties of narrow-bandgap materials have attracted extensive attention worldwide. In this paper, we review the progress of narrow-bandgap materials from many aspects, such as background, nonlinear optical properties, energy band structure, methods of preparation, and applications. These materials have obvious nonlinear optical characteristics and the interaction with the short pulse laser excitation shows the extremely strong nonlinear absorption characteristics, which leads to the optical limiting or saturable absorption related to Pauli blocking and excited state absorption. Especially, some of these novel narrow-bandgap materials have been utilized for the generation of ultrashort pulse that covers the range from the visible to mid-infrared wavelength regions. Hence, the study on these materials paves a new way for the advancement of optoelctronics devices.

Keywords narrow-bandgap materials, saturable absorber, ultrafast lasers, modulator, photodetectors

Contents

1 Background and research progress 1
2 Nonlinear optics of novel NBMs 9
2.1 Optical nonlinear absorption 9
2.1.1 Saturable absorption 9
2.1.2 Anti-saturable absorption 9
2.1.3 Two-photon absorption 9
2.1.4 Carrier absorption 10
2.2 The measurement methods of nonlinear absorption 10
3 The preparation of NBMs 10
3.1 Mechanical exfoliation method 10
3.2 Liquid phase exfoliation method 11
3.3 Liquid phase synthesis method 11
3.4 Chemical vapor deposition (CVD) method 12
3.5 Epitaxial growth (EG) method 12
4 The applications of flexible narrow-bandgap materials 12
4.1 Pulse laser generation based on narrow-bandgap materials 12
4.1.1 Pulsed laser based on graphene SA 12
4.1.2 Solid state laser based on MoS_2 SA 12
4.1.3 Pulsed fiber laser based on BP SA 13
4.1.4 Pulsed fiber laser based on PbS SA 14
4.1.5 Pulsed fiber laser based on bismuthene SA 15
4.1.6 The various pulse laser technologies 17
4.2 Optical modulation based on NBMs 18
4.2.1 The typical methods of optical modulation based on NBMs 18
4.2.2 The typical systems of optical modulation based on NBMs 20
5 Conclusions and outlook 23
Acknowledgements 23
References 23

1 Background and research progress

The NBMs have the layered structure, in which atoms combine with each other through strong chemical bonds and the weak van der Waals force. So, the NBMs have many characteristics different from corresponding block materials. However, different dimensions of carbon structural materials show different properties, such as 0D fullerenes [1], lD carbon nanotubes [2], 2D graphene [3], and 3D graphene. And these materials were found and

#These authors contributed equally to this work.
*Special Topic: Black Phosphorus and Its Analogues (Eds. Xianhui Chen, Haibo Zeng, Han Zhang & Yuanbo Zhang). This article can also be found at http://journal.hep.com.cn/fop/EN/10.1007/s11467-021-1055-z.

studied in chronological order: 3D graphite, 0D fullerenes, 1D carbon nanotubes, and 2D graphene. Hence, narrow-bandgap 2D materials have an attractive application prospect in the field of optics and electronics. There is a quantum limit effect in the vertical narrow-bandgap 2D plane direction, which can be controlled by the number of layers of the material. The bandgap varies widely, which has great potential in the application of broadband response photonic devices. Because of the weak van der Waals force between the layers, NBMs are used to prepare heterogeneous junction materials, and the problems caused by the mismatch of interface lattice can be effectively suppressed. Meanwhile, surface is passivated naturally without suspension bonds due to the van der Waals force between layers, which makes it easier to combine NBMs with photonic devices. This is the reason why NBMs are used in fiber lasers. The technology of employing these narrow-bandgap materials as saturable absorbers (SAs) has promoted the development of ultrafast laser generation. And the structures of these materials are shown in Fig. 1 [4–10].

In 2004, Geim and Novoselov *et al.* reported that graphene [3] was obtained by stripping off with adhesive tape and its related physical properties were studied, which triggered a boom in the research on NBMs worldwide. In 2016, Chernysheva *et al.* used carbon nanotubes (CNTs) in ytterbium (Yb), bismuth (Bi), erbium (Er), thulium (Tm) and holmium-doped fiber lasers to achieve integrated operation in fiber laser cavity, which makes carbon nanotubes make outstanding progress in the application of fiber optics [11]. The valence bands and conduction bands encounter at the Dirac points of the single-layer graphene, which leads to a semi-metallic band structure without the bandgap. Ultrawide band ranging from far-infra-red (FIR) to ultraviolet (UV) region interacts with electromagnetic waves [12–16]. The mechanism of energy level description for various nonlinear optical (NLO) [17–23] processes in graphene is shown in Fig. 2(a) [24–29]. And the Raman spectra and constant spectra of graphene sheets with the different number of layers that measured on quartz are shown in Figs. 2(b) and (c). Figures 2(d)–(f) show the optical contrast spectra in order to identify the thickness of graphene sheets covered on the fiber core area.

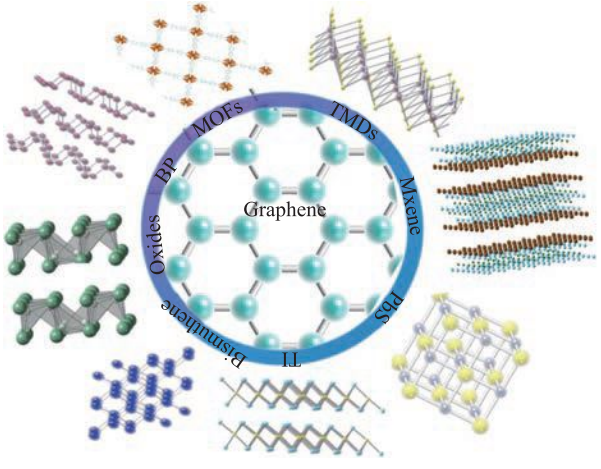

Fig. 1 The current predominant materials as NBMs SA for the generation of ultrashort pulse.

TMDCs, including MoS_2, WS_2, WSe_2 and so on, are another kind of significant narrow-bandgap optoelectronic materials. For several years, the unique optoelectronic properties of TMDCs have led to a worldwide research boom [6, 30–33]. In 2015, Robert *et al.* used MoS_2, WS_2, and WSe_2 to realize its application as a multifunctional, broadband saturable absorption material in fiber laser Q-switching and mode-locking [34]. The expression of transition metal sulfide is MX_2 (M=W, Mo, etc; X=S, Se, or Te). The 3D MX_2 has enormously important properties, such as semiconductor properties, semimetallic magnetism [35], and superconductivity [36]. It can be used as lubricant, catalyst, solar cell, supercapacitor, and rechargeable battery [31, 36–40]. The lattice structure of the layered MX_2 nanosheet is composed of two hexagonal MX_2, with a layer of metal atoms between the two sulfur atoms, forming a sandwich structure. The lattice structures of TMDCs are shown in Figs. 3(a) and (b). Figure 3(c) [31] shows the optical bandgap versus the layer number for the typical TMDCs and other NBMs. MX_2 nanosheets possess many advantages, such as the special electrostatic coupling effect, large carrier mobility, high-intensity current storage characteristics, strong visible absorption, and good chemical and mechanical properties [42–45]. Therefore, MX_2 nanosheet can be applied in many fields, such as effect transistor [46–49], photoelectric transistors [50, 51], integrated circuit [52], chemical sensors [53], light-emitting diodes [54], and solid-state laser devices [55–61].

The emergence of a novel NBM black phosphorus (BP) [62] fills the gap between graphene and TMDCs (0–1 eV). The bandgap of BP can be adjusted from 0.3 to 2 eV [7, 63] with the decrease of the number of layers. As a kind of excellent 2D material, BP nanosheets can be applied to electronic equipment. The field effect transistors made by BP also have some attractive features, such as an on-off ratio of 10^5 (ultrathin equipment) at room temperature, excellent current saturation characteristics, about 1000 $cm^2 \cdot V^{-1} \cdot s^{-1}$ (10 nm thick BP) field effect electron mobility [64]. Therefore, the BP has a broad range of latent applications in the field of photonics [65–72], such as infrared band luminescence, light detection and modulation [73–75].

The monolayer BP nanosheet has direct bandgap and high charge mobility, which makes it widely used in the field of 2D photoelectricity. Figures 4(a) and (b) show the optical absorption of various layers of BP along the x and y directions, respectively [76]. Continuous modulation of the bandgap of BP nanosheet can be achieved by external

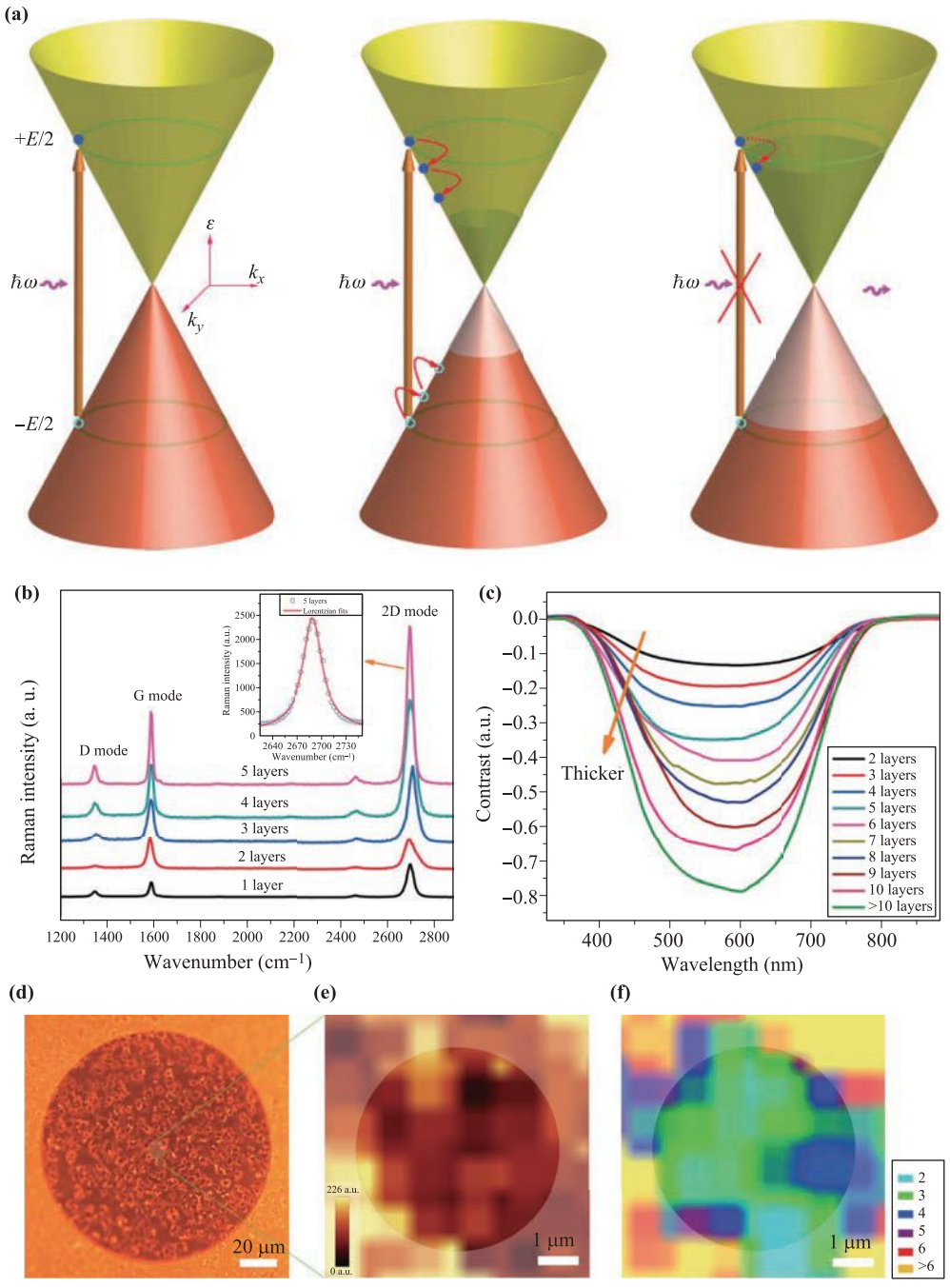

Fig. 2 **(a)** The schematic of energy level for different nonlinear optical processes of graphene **(b)** Raman spectra, and **(c)** contrast spectra of graphene sheets with different thickness measured on quartz. **(d)** Optical image of fiber pigtail end. **(e)** Raman image around fiber core. **(f)** Optical contrast image exhibiting 2–4 layers graphene coated on fiber core. Reproduced from Ref. [12].

stress or external electric field [77], which can be applied in solar cells, photonics devices, etc. [78, 79].

Topological insulators (TIs) of group V chalcogenide also possess a layered structure with the large interlayer van der Waals gap. And TI is a 2D photoelectric material with internal insulation and electric conduction at the surface or edge. TI has a Dirac cone structure similar to graphene [80] due to its strong spin orbit coupling. In the body of TI, the electron energy band structure is similar to the conventional insulator, and the Fermi energy level is between the conduction band and valence band. The surface state is determined by the topological structure of its body electron state and is hardly affected by impurities and disorder, so it is very stable. The surface state structure of TI is similar to graphene energy band structure, which has no bandgap and the inverted

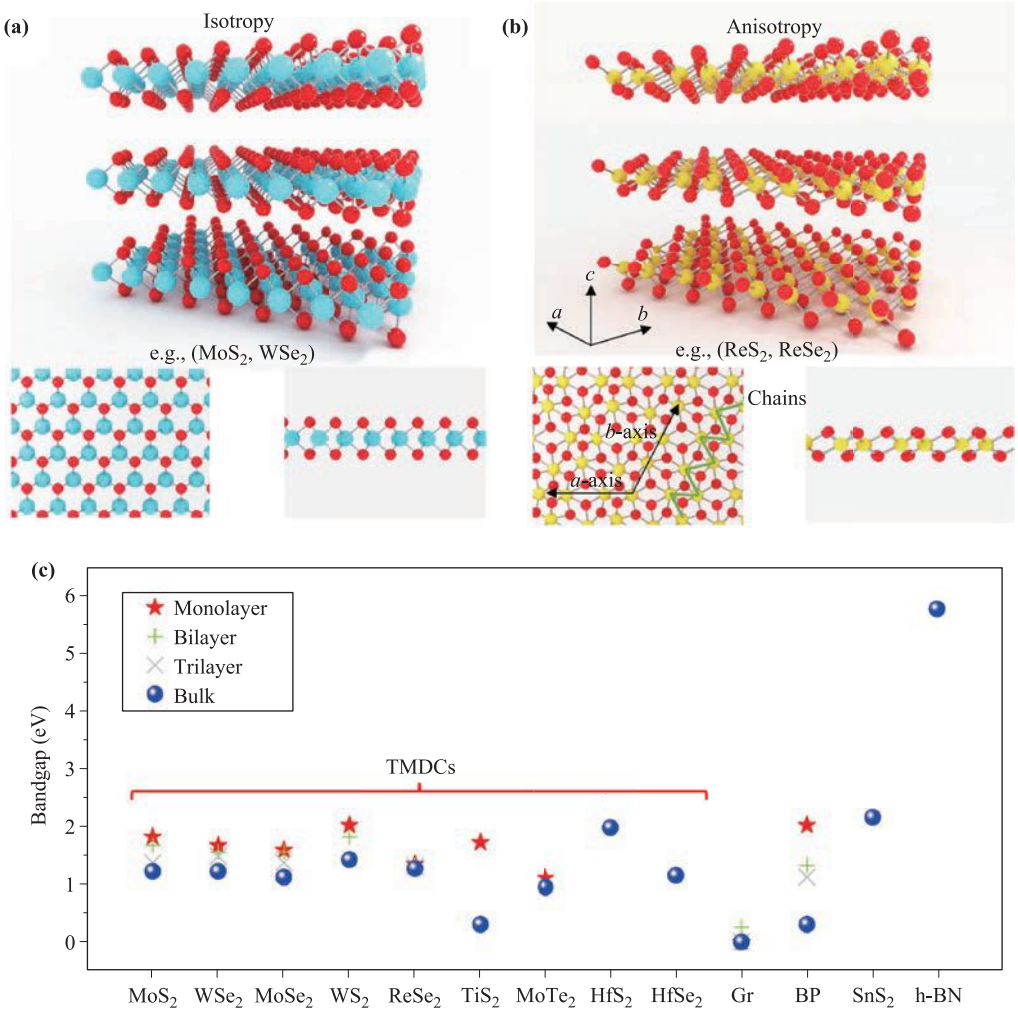

Fig. 3 **(a)** Typical isotropic and **(b)** typical anisotropic sandwich structure of TMDCs. **(c)** The optical bandgap versus the layer number for typical TMDCs and other NBM. Reproduced from Ref. [31].

cone intersects with the Dirac point. In 2013, the phase diagram evolution of the dynamical properties of Dirac fermions with doping content was established by Chen *et al.* [81], as shown in Fig. 5(a). And Fig. 5(b) shows the evolution of surface state band structure and electron self-energy with the composition in $Bi_2Te_{3-x}Se_x$ system. Up to now, the strong TI materials have been confirmed by experiments including Sb_2Se_3, Bi_2Se_3, Bi_2Te_3, Sb_2Te_3, etc. These materials are protected by time inversion symmetry so that they can resist disorder effects and local disturbance. Hence, these materials have potential applications in the field of electronics and optoelectronics [82–89].

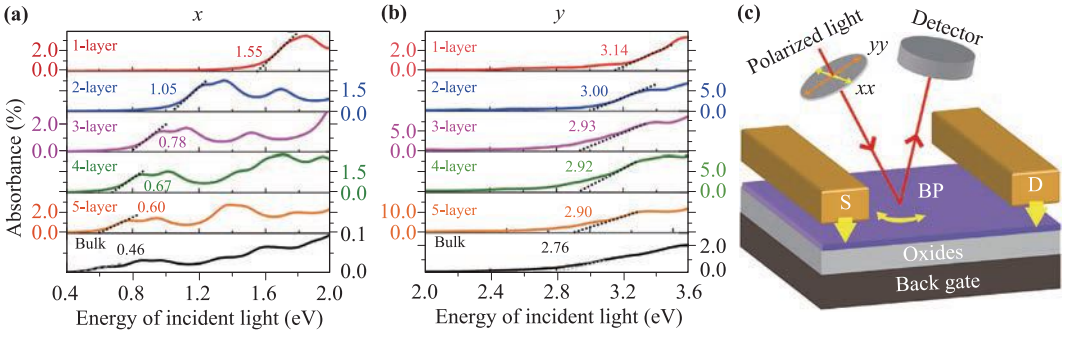

Fig. 4 Optical absorption spectra of different layers of BP along the x direction **(a)** along the y direction **(b)**. **(c)** Schematic diagram of the proposed geometry. Reproduced from Ref. [76].

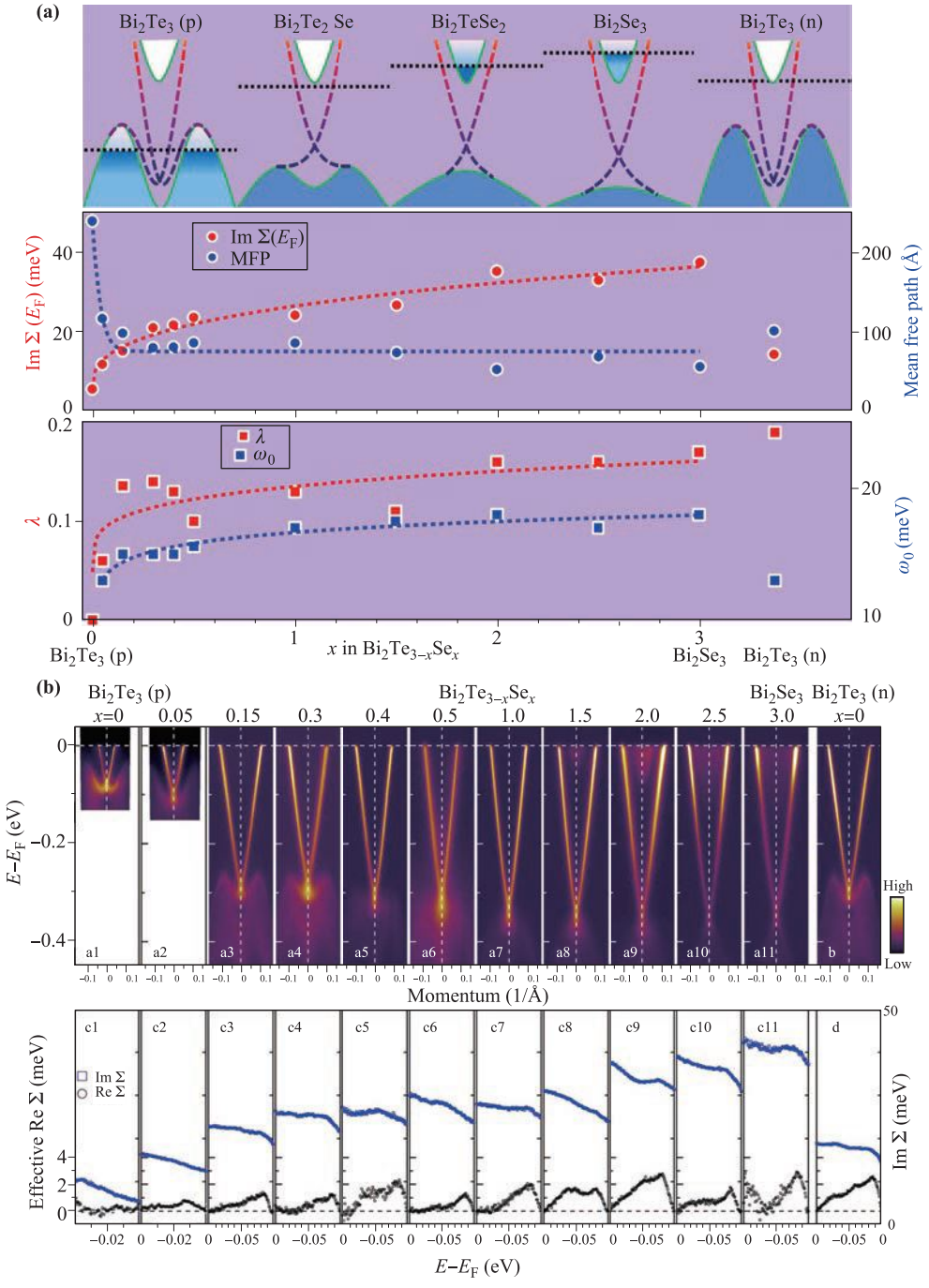

Fig. 5 **(a)** Topological insulator $Bi_2(Te_{3-x}Se_x)$ surface state electrophonon interaction and electron impurity scattering with the evolution of components. **(b)** Evolution of the surface state band structure and electron self-energy in $Bi_2(Te_{3-x}Se_x)$ system. Reproduced from Ref. [81].

In recent years, bismuthene has attracted much attention because of its unique electro–mechanical properties and excellent stability [90–93]. Bismuthene as a kind of excellent candidates for the application of spintronic devices does not require strong external magnetic field on account of its inherent spin–orbit coupling features [94, 95]. It also has semi-metallic properties in comparison with the metal materials, and its long Fermi wavelength of electronic properties is conducive to the research in the field of condensed matter physics [96, 97]. If the bismuthene turns narrower than the Fermi wavelength, the transform from the semimetal to semiconductor may occur due to quantum confinement effects [98]. Figure 6(a) exhibits the diagram of the saturable absorption of bismuthene [99]. In order to obtain the saturable absorption of bismuthene, the intensity ought to completely fill the lower energy level to attain the standard of photon excitation. The optical absorption spectra of few-layer bismuthene solution is shown

in Fig. 6(b), and the inset is the amplified NIR absorption region. And the UV-vis-NIR spectrum is shown in Fig. 6(c) [99].

Since 2004, when monolayer graphene was discovered by the scientists at the University of Manchester in the UK, graphene has caused a worldwide research boom. The nonlinear optical properties of graphene and its applications in passively Q-switched, mode-locked lasers and optical limiters are also widely studied. In 2009, Wang *et al.* [98] from Dublin Trinity College discovered that graphene dispersion had an anti-saturation absorption effect under the radiation of 532-nm and 1064-nm nanosecond pulse, and they had explained that the principle came from the nonlinear scattering of the solution. In the same year, Bao *et al.* [26] achieved the saturable absorption of the low-layer graphene nanosheet under the femtosecond pulse of 1550 nm for the first time, which realized successfully the mode-locking output pulse in the fiber laser. In 2010, Yu *et al.* [101] of Shandong University reported the saturable absorption characteristics of graphene in the 1.34 μm band and realized the application of Q-switching in the solid-state laser. Subsequently, the researchers also realized the saturable absorption characteristics of graphene in the visible-ultraviolet-near infrared and even in the terahertz band. The tunable ultrafast mode-locked and Q-switched laser output in broadband can be achieved based on this material [102–104]. In addition, the third-order nonlinear refractive index coefficient of graphene has been reported. In 2010, the nonlinear optical properties of graphene were explored using the four-wave mixing method by Hendry *et al.* [105] from the University of Exeter, and they pointed out that the third-order nonlinear polarization rate of graphene under the action of picosecond pulse in near-infrared band is eight orders of magnitude higher than that of dielectric material. Subsequently, the researchers used nanosecond and femtosecond lasers to obtain the nonlinear refractive index and polarization rate of graphene, which was several orders of magnitude higher than that of general medium materials under the same experimental conditions [106, 107].

With the boom of graphene research, the graphene-like nanomaterials also come into researchers' view. TMDCs are a kind of graphene-like nanomaterials, and single-layer structure of TMDCs has high-intensity photoluminescence characteristics in terms of optical properties. Moreover, theoretical calculations prove that single-layer TMDCs have unique photoelectron characteristics, and their exciton has selectivity, super-strong exciton binding energy and stress controllable banding width in the Brillouin energy valley. Therefore, the third-order nonlinear optics of TMDCs has aroused great interest in recent years. In 2013, Wang *et al.* [108] of Shanghai Institute of Optics and Fine Mechanics studied the saturable absorption characteristics of the few-layer MoS_2

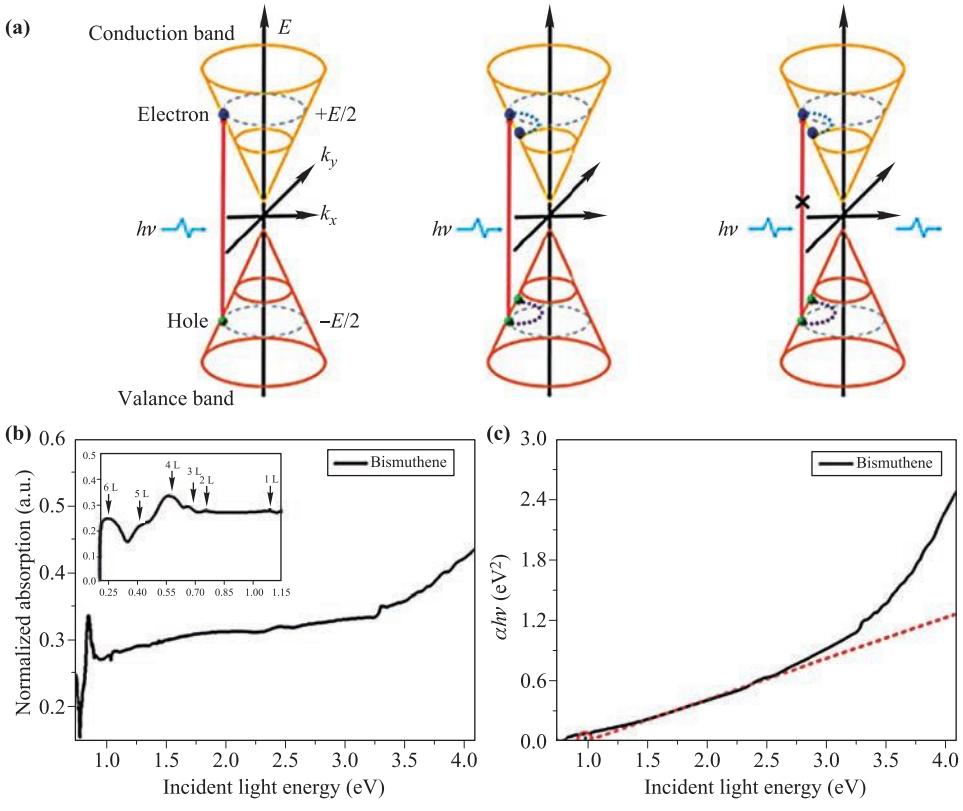

Fig. 6 **(a)** The schematic diagram of saturable absorption of bismuthene. **(b)** The optical absorption spectrum. **(c)** The UV-vis-NIR spectrum of the few-layer bismuthene. Reproduced from Ref. [99].

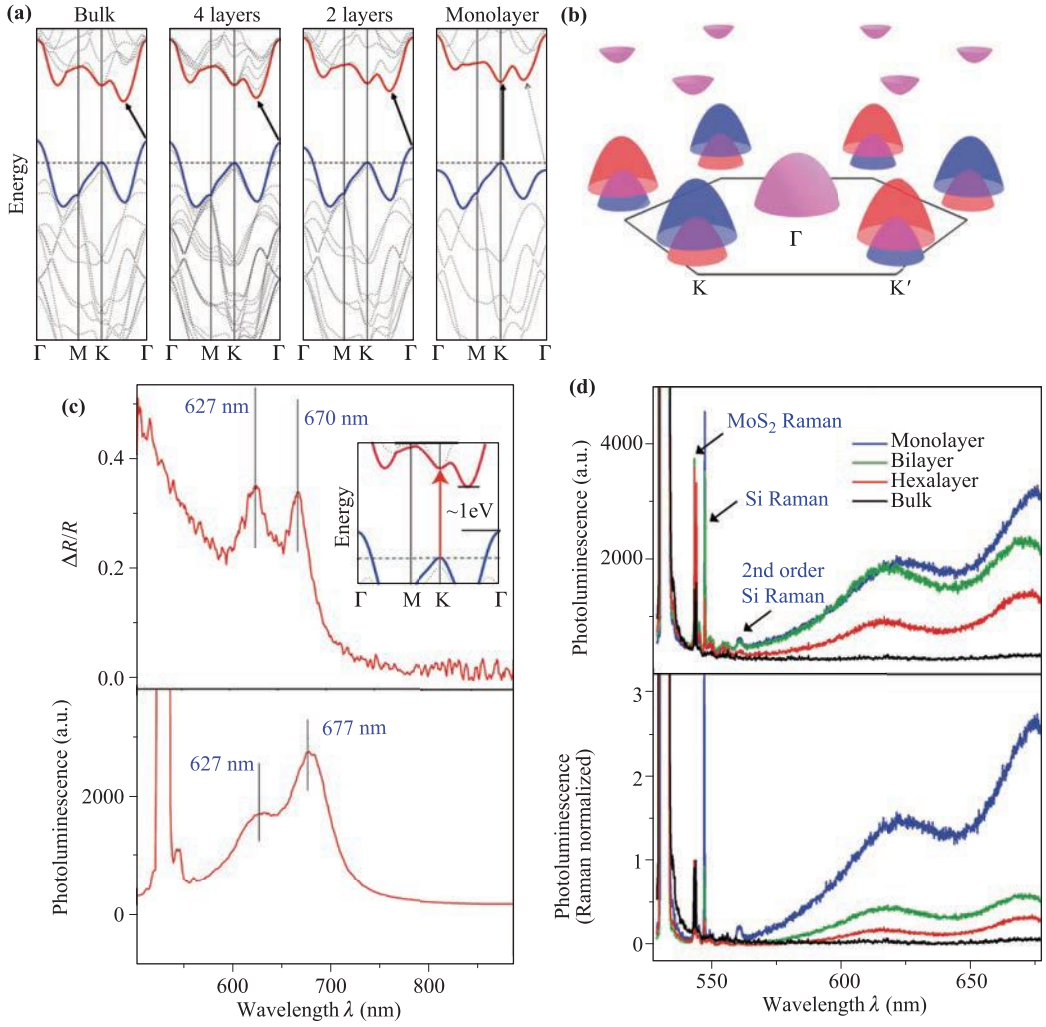

Fig. 7 **(a)** Evolution of the band structure. **(b)** Schematic diagram of the band structure of monolayer MoS_2. **(c)** The reflection and photoluminescence spectra of ultrathin MoS_2 layers. **(d)** Layer dependence of photoluminescence efficiency in MoS_2 with different thickness. (a, c, d) Reproduced from Ref. [110], (b) Reproduced from Ref. [111].

dispersion under the action of femtosecond laser at 800 nm band for the first time. The results showed that the saturable absorption performance of MoS_2 dispersion under the same experimental conditions is better than that of graphene dispersion with the same concentration. In 2016, the nonlinear optical characteristics and physical mechanism of TMDCs had been further systematically studied by this research group, and the nonlinear optical functional control and shear strategy of such materials also have been proposed and verified [109]. Figure 7(a) shows the calculated band structures of TMDCs, such as bulk MoS_2, quadrilayer MoS_2, bilayer MoS_2, and monolayer MoS_2 [110]. The spin splitting of the bands at the K and K′ points on the corners of the Brillouin zone [55, 111] is exhibited in Fig. 7(b), and the colors of orange and blue indicate up and down spin polarization. The reflection and photo-luminescence spectra of ultrathin MoS_2 layers are shown in Fig. 7(c) [110]. And the layer dependence of photo-luminescence efficiency in MoS_2 with the different thickness is exhibited in Fig. 7(d). In 2014, Zhang *et al.* [55] of Shenzhen University confirmed that single-layer MoS_2 has nonlinear optical characteristics from visible to near-infrared band, and successfully realized the mode-locked ultrashort pulse laser output in the near-infrared band based on this material. In the same year, Cheng *et al.* [112] from Harbin Engineering University reported that the nonlinear characteristics of MoS_2 can shift from saturable absorption to anti-saturable absorption with the increase of power. Meanwhile, Zhang *et al.* [113] of Lanzhou University prepared the different sizes of TMDCs by using the method of distributed centrifugation, and obtained that the nonlinear optical properties are directly related to the sizes of materials.

In 2015, Mao *et al.* [114] reported that the few-layer WS_2 nanosheets obtained by liquid phase method have the characteristics of saturable absorption and can be applied in the mode-locked laser. Qiu *et al.* [115] of Zhejiang University prepared the few-layer MoS_2 nanosheets

with high yield and uniform thickness by hydrothermal method, which proved its saturable absorption characteristic in the band of 800–1550 nm, and they also achieved Q-switched laser output in the near-infrared band based on this material. Subsequently, in order to achieve excellent Q-switched pulse laser output, the optical absorption rate of the material was enhanced by changing the morphology, and atoms and other methods were added to enhance the saturable absorption performance of materials. In addition, this research group used solid phase method to synthesize ultrathin MoS_2 and WS_2 nanosheets, which realized its optical limiting effect at the band of 800 nm, and its optical limiting threshold was much lower than that of traditional optical limiting materials.

With these materials emerging subsequently, the TIs also come into researchers' horizons. In 2012, Bernard *et al.* [116] of the Brussels Free University of Belgium first realized the saturable absorption characteristics of the topological insulator Bi_2Te_3 in the communication band. In the same year, Wen *et al.* [117, 118] took the lead in utilizing the saturable absorption characteristics of two TI materials, Bi_2Se_3 and Bi_2Te_3, to realize the mode-locked pulse output in the fiber laser. In 2013, this group measured the nonlinear refractive index [119] of Bi_2Se_3 by Z-scan method under the action of near-infrared femtosecond laser for the first time. In 2014, Jung *et al.* [120, 121] realized the applications of passively mode-locked and Q-switched lasers in the 2 μm band based on TIs materials. In 2016, the researchers in Zhejiang University prepared Bi_2Te_3 nanosheets with high yield and uniform size and thickness by adding surfactant PVP into the solvent thermal method. The output performance of Q-switched laser output was obtained based on TI by using this method, which is superior to TI made by liquid phase stripping. Meanwhile, a ternary topological insulator Bi_2SeTe_2 possessing excellent saturable absorption performance was prepared by solvent heating method and the theoretical work verified the performance [83].

Recently, many researchers have paid attention to novel diazo-metal-elements materials such as As, Se, and Bi [122, 123] with the rapid development of these flexible NBMs. The bismuthene has the semimetallic features and narrow-bandgap of 0.4 eV with single-layer structure [124, 125]. And the bismuthene can be translated from semimetal into semiconductor on account of the effect of quantum confinement. In 2016, Zhang *et al.* [126] investigated the arsenene, phosphorene, antimonene and bismuthene that have the high carrier mobility and the narrow bandgap. In 2018, Lu *et al.* [99] reported a ring cavity fiber laser based on bismuthene with the modulation depth of 2.03% and experimentally achieved conventional solitons with the pulse duration of 652 fs, which shows that bismuthene is a novel narrow bandgap material for the ultrafast photonics. In the same year, Yang *et*

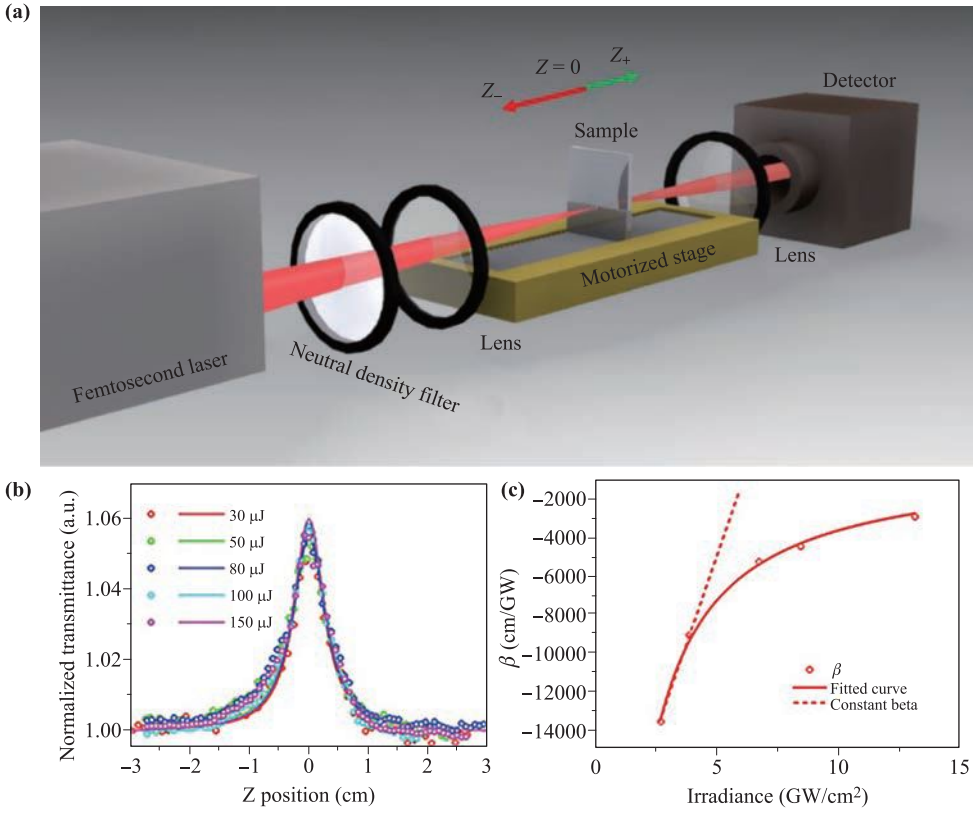

Fig. 8 **(a)** Open Z-scan experimental device. **(b)** Nonlinear absorbance measured by the Z-scan system. **(c)** Fitting curves of the nonlinear coefficient. Reproduced from Ref. [176].

al. [127] reported a Tm-doped fiber ring cavity laser and successfully obtained a 2 μm output with pulse duration of 1 ns. Chai and Wang *et al.* [9, 10] also reported the Yb-doped fiber laser and Er-doped fiber laser based on bismuthene, respectively.

The unique optic–electronic properties of these narrow bandgap materials [128–130] enable them to have great application prospects in the construction of micro-nano opto–electronic devices.

2 Nonlinear optics of novel NBMs

The third-order nonlinear optical properties of NBM have been a hot research area for several years, including saturable absorption, anti-saturable absorption, and so on. The saturable absorption describes that the optical absorption rate of a material decreases with the enhancement of incident light and eventually becomes a constant. A material with the saturable absorption property can be regarded as SA and used as passively mode-locked or Q-switched element in the fiber lasers [131–136]. Since its emergence, the laser has been moving toward the direction of tunable, short pulse and high energy output. The passively mode-locked technique uses saturable absorption characteristics to realize the continuous narrowing of the pulse duration, thus generates the required ultrashort optical pulse [137–140]. The passively Q-switched technique [141–144] is used to insert the Q-switched element with fixed parameters into the laser cavity, and the saturable absorption characteristic of the Q-switched elements is used to adjust the Q-value. When the stimulated radiation occurs, the inverted particles stored in the high energy level of the gain fiber can quickly transit back to the low energy level and release huge amounts of energy in a very short time, which can result in high-energy pulse output.

At present, the most widely used SA is the semiconductor SA [145–150]. However, there are some disadvantages such as high price, complicated production process, narrow wavelength range, and low output energy. Therefore, it is very important to find a SA with advantages of broadband tunable nonlinear absorption, ultralow loss, high damage threshold, ultrashort response time, high modulation depth and ultralow cost. As a novel kind of materials, narrow-bandgap photoelectric materials have unique saturable absorption properties, which have a good application prospect in pulsed laser generation. Moreover, narrow-bandgap photoelectric materials also have unique anti-saturable absorption properties, hence, it has potential applications in laser limiting.

2.1 Optical nonlinear absorption

Light absorption is a fundamental interaction between substance and light. And it can be divided into linear absorption and nonlinear absorption. A phenomenon in which the absorption coefficient of a substance varies with the intensity of incident light is called nonlinear absorption, and the opposite is the linear absorption. Nonlinear absorption is a nonlinear effect under the action of highly coherent light, which has been widely studied. Due to different absorption mechanisms of substance, nonlinear absorption can be divided into saturable absorption [151–155], anti-saturable absorption, two-photon absorption, and carrier absorption. The saturable absorption and two-photon absorption are the most important and common nonlinear absorption effects. These nonlinear absorption properties are as follows.

2.1.1 Saturable absorption

When the intensity of excited light reaches a certain value, the phenomenon that the absorption coefficient of the material decreases instead of increases is called saturable absorption, which is mainly caused by the principle of Pauli incompatibility. When the excitation intensity is weak, the electrons in the valence band absorb the photon energy and are excited to the conduction band. At the same time, they are gradually cooled and arranged due to the restriction of the Pauli Exclusion Principle. When the electron energy state in the Fermi level is filled, the incident intensity is called saturable intensity. As the light keeps on increasing, the redundant photons will no longer be absorbed by the electrons in the valence band, but move transparently through the acting medium.

From the macro perspective, the light transmittance will gradually increase when the energy of the excitation light increases. When the energy reaches the saturable intensity, the transmittance will no longer increase but gradually move to a stable value. This nonlinear effect is widely used in solid-state and fiber mode-locked lasers or passively Q-switched lasers [156–165].

2.1.2 Anti-saturable absorption

Contrary to the saturable absorption, the absorption coefficient of the medium increases in accordance with the increase of light intensity. The mechanism is that the electrons in the low energy state are excited and then jump to the high energy electron state. When the absorption crosses the section of the excited state is more excellent than the absorption cross section of the ground state, which is called the reverse saturation absorption. From the macro perspective, under high power laser excitation, the transmission rate of medium decreases instead of increases, which can be used in the optical limiting devices.

2.1.3 Two-photon absorption

Two-photon absorption refers to the process in which the medium energizes or combines two photons of the same energy or different energy to excite the electrons in the low energy state of the valence band to the high energy

state under strong light excitation. It is important to note that the two photons absorbed can be the same photons or different photons. In the excitation process, the electron absorbs a single photon and is excited to a virtual electron state, almost simultaneously. And another photon is absorbed by the same electron and is excited to a higher excited state. Since the interval is very short, we can think of two photons being simultaneously absorbed and excited to a high energy state. Similar to the anti-saturable absorption, this phenomenon is also applied to optical limiting devices [27, 166–173].

2.1.4 Carrier absorption

When the frequency of incident light is less than the bandwidth of the semiconductor, electrons cannot form an energy band transition, and electrons absorb photons to form free carriers (electrons or holes) at the same time. The free carrier is still restrained by the surrounding charge, but it is in an excited state. When the frequency of incident light is greater than the band width of the semiconductor and the energy transition occurs (saturable absorption or two-photon absorption), the electron excited to the conduction band cannot exist and also forms a large number of free carriers. These carriers continue to absorb photon energy, and they are excited to other energy levels as carriers.

2.2 The measurement methods of nonlinear absorption

The methods of measuring nonlinear absorption characteristics of materials include nonlinear interferometry [174], four-wave mixing, three-wave mixing [175], ellipsometry, beam distortion and Z-scan. Although the first three methods are highly precise, the required equipment is very complex and expensive, and the calculation of ellipsometry is relatively complicated. The beam distortion method is very strict and has large errors. The experimental equipment and analysis required by Z-scan is relatively simple and the data is relatively accurate. Hence, this is the main experimental method described in this paper.

The Z-scan method was first adopted by Sheik–Bahae *et al.* in 1989. In the following years, they gradually improved this method and launched corresponding theoretical model to figure out the nonlinear refractive index and nonlinear absorption coefficient of substances. This method is very simple and flexible and the data is considerably accurate. Hence, it is quickly accepted by researchers, and has been rapidly developed and improved. The open Z-scan method is mainly used to measure the nonlinear absorption performance of the materials. Figure 8(a) shows the commonly used Z-scan experiment device [176]. The type of the excitation laser light source has a wavelength of 1030 nm. The excitation pulse width is 340 fs and the frequency is 100 Hz. The beam waist radius is about 32 μm at 1030 nm. The beam is focused through focal length lens. Behind the lens is a moving platform, and the center of the moving platform is near the beam waist of the laser beam. The sample can be moved in the axial direction of the beam by moving the platform. The laser is divided into two beams with equal energy using a beam splitter, then the incident and output energy of the sample are recorded in real time with two energy meters and transmitted the data to the computer for analysis. The normalized transmittance curves with the different testing energy values are shown in Fig. 8(b), which indicates clear saturable absorption responses in the different energy values, and the SA performance exhibits the excellent stability with the increase of pulse energy. The fitting values of the nonlinear coefficient and their fitted curves are shown in Fig. 8(c).

As seen in Fig. 8(a) [176], the power density of the incident laser is low when the sample is far away from the beam waist. At this time, the absorption form of the sample is mainly linear absorption with little change in transmission energy. As the sample gets closer to the beam waist, the incident optical power density increases gradually, and the sample will show nonlinear absorption effect. When the output energy curve presents a symmetric wave peak, it indicates that the sample has a saturable absorption effect, as shown in Fig. 8(b). In contrast, when the output energy curve is a symmetrical wave trough, the sample is reflected as the optical limiting effect. Notably, in the Z-scan measurement, the thickness of sample used in the experiment is smaller than the Rayleigh length of the beam. When a moderate aperture is added to the back of the sample, we call it a closed aperture Z-scan. Combined with the results of an open Z-scan, the nonlinear refractive index of the sample can be obtained.

3 The preparation of NBMs

The development of batch manufacturing methods of high-quality NBMs is the key and foundation to realize the in-dustrial application of optoelectronic devices. Generally, the preparation methods of NBMs are divided into top-down method and bottom-up method. The top-down method includes mechanical exfoliation method and liquid phase exfoliation method. While the bottom-up method includes liquid phase synthesis, chemical vapor deposition (CVD), epitaxial growth (EG) and other methods. Here are some common methods of stripping and synthesizing NBMs [177–180].

3.1 Mechanical exfoliation method

In 2004, Geim and Novoselov *et al.* [1] were the first to realize the preparation of monolayer graphene by solid-phase mechanical exfoliation. Some scaly debris can be obtained by rubbing the surface of the layered material, and there are even NBMs with a monolayered structure in this detritus. The general way is to press the tape paper onto the surface of the corresponding block ma-

terial, and NBMs will be attached to the surface of the tape paper after removing the tape paper. The NBMs obtained by this method have a high degree of crystal crystallization and can be easily screened out by an optical microscope. Through further tests, for example, scanning electron microscopy (SEM), high resolution transmission electron microscopy (HRTEM), transmission electron microscopy (TEM), and atomic force microscopy (AFM), more information about its morphology, thickness, and size can be revealed. Due to the common structural features of the weak van der Waals binding between layers of NBMs, the mechanical exfoliation method is also applicable to the preparation of other graphene-like NBMs. In this way, many layered and crystalline materials can be stripped out, such as boron nitride (BN), MoS_2, $NbSe_2$, $MoSe_2$, WS_2, WSe_2, and Bi_2Te_3 [180–183].

The advantages of this method are simple operation, high efficiency, low cost, and wide adaptability. The size of single-sheet NBMs can reach tens of microns in the transverse, and possess better crystallization and surface cleanliness. Hence, it has excellent photoelectric properties. However, this is a relatively original method that was first used to strip graphene. Its obvious disadvantage is that the samples obtained by this method are mostly multilayer structures, and has less samples with few-layer or single-layer structures. This method cannot realize the mass production of NBMs and cannot meet the needs of the industry.

3.2 Liquid phase exfoliation method

In 2010, Ruoff *et al.* [184] reported for the first time that the high-performance preparation of graphene oxide (GO) was achieved by liquid phase exfoliation method, and graphene could be obtained more efficiently by subsequent reduction. Since then, researchers have conducted extensive research on the impact of the solution on the effect of liquid phase exfoliation graphene and developed a more systematic theory [185–188]. In this method, many researchers realized the preparation of TMDCs (such as WS_2, MoS_2, $MoSe_2$, $TaSe_2$, $MoTe_2$, and $NbSe_2$), BP, TIs, h-BN dispersion recently [179, 189–194]. Liquid phase exfoliation is a method of dispersing LBM powders in specific solvents and peeling LBM from the surface of the corresponding powder particles by means of high power ultrasonic vibration.

The common solvent is anhydrous, but ultra-pure water solutions are also available for some materials. Under the action of solvent, the LBM is separated into small structural units. After a long period of stasis, the NBMs dissolved in the solvent will be stratified, and the larger particles will gradually precipitate. The upper suspension contains a large number of single-layer or multilayer narrow-bandgap nanoparticles. In addition, the whole stratification process can be accelerated by centrifugal action.

The advantages of this method are simple, safe, low cost, and suitable for mass production. The surface of materials can be chemically modified at the same time. While the drawback is that the NBMs obtained are irregular in shape and not uniform in thickness, and the physical and chemical properties are easily changed due to the action of surface dispersion.

3.3 Liquid phase synthesis method

The liquid phase synthesis method takes water or other organic solvents as reaction medium to dissolve or disperse the particles of NBMs. It can realize the crystallization and growth of NBMs in the reaction medium under heating and (or) high pressure conditions, and separate the products through precipitation, centrifugation, washing, drying and other steps after the end of the reaction. This method regulates the growth, shape, size and sur-

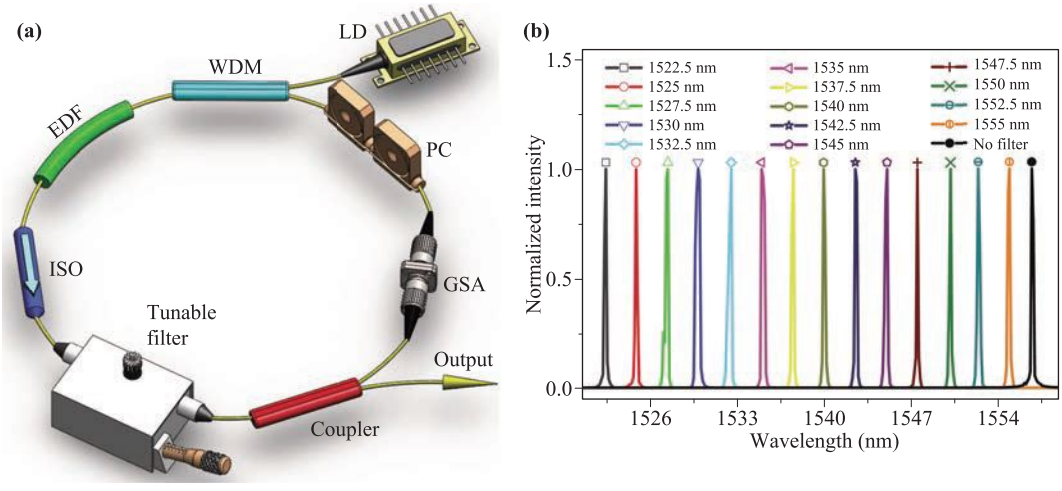

Fig. 9 **(a)** Experimental schematic diagram of ultrafast fiber lasers. **(b)** The wideband adjustable output spectra near the telecommunication band in the Q-switched fiber laser based on graphene. Reproduced from Ref. [224].

face chemistry of crystals by adding the specific surfactant (such as PVP) in the reaction solution and controlling the reaction temperature, reaction time, etc., which can obtain various shapes of nanosheets and nanobelts [37, 38].

Generally, the advantages of this method are that the product has good crystallization and it can realize the mass production. But it is difficult to obtain single layer NBMs, and its production needs longer reaction time. Most importantly, the liquid phase reaction will inevitably adsorb surfactant and other substances on the surface of the product, which will have the certain impact on the properties of the material itself [40, 41, 195].

3.4 Chemical vapor deposition (CVD) method

Currently, the large area uniform NBMs (like graphene) can be synthesized by chemical vapor deposition method, which shows good commercial prospects. And CVD method is the most widely used technology to prepare high-quality NBMs (especially graphene). CVD method is a preparation technique for the formation of target material by chemical reaction on the substrate surface under the action of heat, laser, plasma and another additional energy, and it is of great importance and can be applied in many fields such as optoelectronic devices and semiconductor industry. The most typical example of NBMs produced by CVD is the preparation of high-quality graphene materials [5, 178, 196–198]. Although the mechanical exfoliation method can get high-performance few-layer and single layer graphene, it cannot be applied to the industrial production.

However, the CVD method cannot realize the low-cost production of large-size and high-quality graphene [5, 199–201], researchers have successfully prepared monolayer, double-layer and multilayer graphene of wafer scale, which are widely used in flexible transparent optoelectronic devices. CVD technology also shows great potential in the preparation of TMDCs, and researchers have successfully achieved controlled growth of high quality TMDCs on a variety of substrates [202–205]. The merit of this method is that it can get the shapes of sample that people need [206–211]. It requires much energy to grow NBMs based on this method, so the damage rate of growth on copper substrate sheet is relatively higher. And partial inhomogeneity still exists in NBMs grown by this method.

3.5 Epitaxial growth (EG) method

The epitaxial growth method is a technique for growing high quality thin films on crystalline substrates [212]. Under the condition of ultrahigh vacuum, the precursor steam is produced by the heat evaporator with various kinds of precursor materials, which is collimated through the holes to form the molecular beam or atomic beam, and then sprayed to the single crystal substrate at the appropriate temperature [213, 214]. By controlling the molecular beam or atomic beam to scan the substrate, the molecules or atoms can grow on the substrate layer by layer according to the crystal arrangement [215].

The obvious characteristic of EG method is that the deposition rate is very slow, and it can prepare highly crystalline film with crystal growth orientation, controllable composition and precisely adjustable thickness. The merit of this method is that it can produce high quality semiconductor heterojunctions or superlattices by periodically turning on or off the specific evaporation sources. Hence, this is a very important preparation method in the semiconductor industry [216, 217].

4 The applications of flexible narrow-bandgap materials

4.1 Pulse laser generation based on narrow-bandgap materials

4.1.1 Pulsed laser based on graphene SA

Graphene SAs have made the generation of pulsed laser from the visible to infrared range on account of their ultrafast recovery time, ultrawide nonlinear optical response bandwidth and super saturable absorption [24, 218–221]. Bao *et al.* firstly obtained mode-locked operation based on graphene SA in an Er-doped fiber laser (EDFL) that is operated at 1565 nm with the output pulse width of 756 fs [222]. In 2012, mode-locked operation in a mid-infrared (MIR) fiber laser based on graphene SA was reported by Zhang *et al.* for the first time [223]. The solid state lasers [103] have been successfully achieved in the infrared region with the evolution of pulse laser based on graphene SA. The experimental schematic diagram for ultrafast fiber laser is shown in Fig. 9(a) [224]. SAs based on graphene have been applied for the generation of microsecond pulse from NIR to MIR lasers. Figure 9(b) exhibits the adjustable output spectra from Q-switched fiber laser near the third low loss telecommunication wavelength based on graphene SAs [224].

4.1.2 Solid state laser based on MoS_2 SA

With the successful achievement of pulse lasers employing graphene SA, there has been an enormous number of descriptions on the pulsed lasers applying narrow-bandgap semiconductors of dichalcogenides of Mo, such as MoS_2. And for the monolayer MoS_2 whose bandgap is 1.8 eV corresponding the wavelength of 689 nm, because the exit of the edge state and the defect state conduces to the operation of MoS_2 SA in the NIR and MIR, it allows the description of fiber lasers at the wavelengths far longer than the fundamental exciton absorption wavelength [225]. Wang *et al.* [226] were the first group to demonstrate a solid state pulsed laser based on the MoS_2 SA using the bulk

Q-switched cavity. In 2016, Chen *et al.* found hot excitons form quickly after charge transfer based on the MoS_2/WS_2 heterostructure material [227]. The schematic instructions of ultrafast visible and IR microspectroscopy are shown in Fig. 10(a). Figure 10(b) exhibits the image of the transient absorption change for a MoS_2/WS_2 heterostructure material. Figures 10(c) and (d) show the evolution of the absorption changes in WS_2 monolayer (in blue), MoS_2 monolayer (in red), and the MoS_2/WS_2 heterostructure (in green). The signal of the MoS_2/WS_2 heterostructure and the sum of the WS_2 and MoS_2 monolayers are shown in Fig. 10(e).

In 2017, Yan *et al.* found that WS_2 SA displayed excellent nonlinear optical properties and was applied for the generation of ultrafast pulses, as shown in Fig. 11 [228]. Nonlinear absorption curve of few-layer WS_2 and the construction of the fiber laser based on few-layer WS_2 SA are exhibited in Figs. 11(a) and (b), respectively. Figures 11(c)–(f) show the output power, output spectrum, RF spectrum and the autocorrelation trace, respectively.

In 2014, Luo *et al.* rapidly extended the operation wavelength of Q-switched laser based on MoS_2 SA up to 2 μm region [61], and this proposed laser can achieve the higher output power and the lower repetition rate in comparison to others reports based on MoS_2 SA [286]. The mode-locked pulse still can not be generated in solid state lasers based on a bulk-cavity due to the high nonsaturable loss of MoS_2 SAs, but it can be obtained in the fiber lasers. The mode-locked pulse in a Yb-doped fiber laser based on MoS_2 SA was first obtained by Li *et al.* [229] with the center wavelength of 1070.5 nm, the pulse width of 726 ps and the output spectrum bandwidth of 1.7 nm. And this fiber laser system has many advantages, such as flexible maneuverability, compact construction, and low cost characteristics, which make this system compatible and flexible for applications in reality.

4.1.3 Pulsed fiber laser based on BP SA

The emergence of BP fills the gap between graphene and TMDCs (0–1 eV). The bandgap of BP can be adjusted from 0.3 eV (multilayer) to 2 eV (single layer) with the decreasing number of layers, which can be applied in the field of ultrafast photonics [230–234]. BP shows unique electric and optical properties, which can be regarded as the excellent SA for the applications of NIR and MIR region. Chen *et al.* [165] firstly reported BP SA in a communication band of 1550 nm. And the SA was made

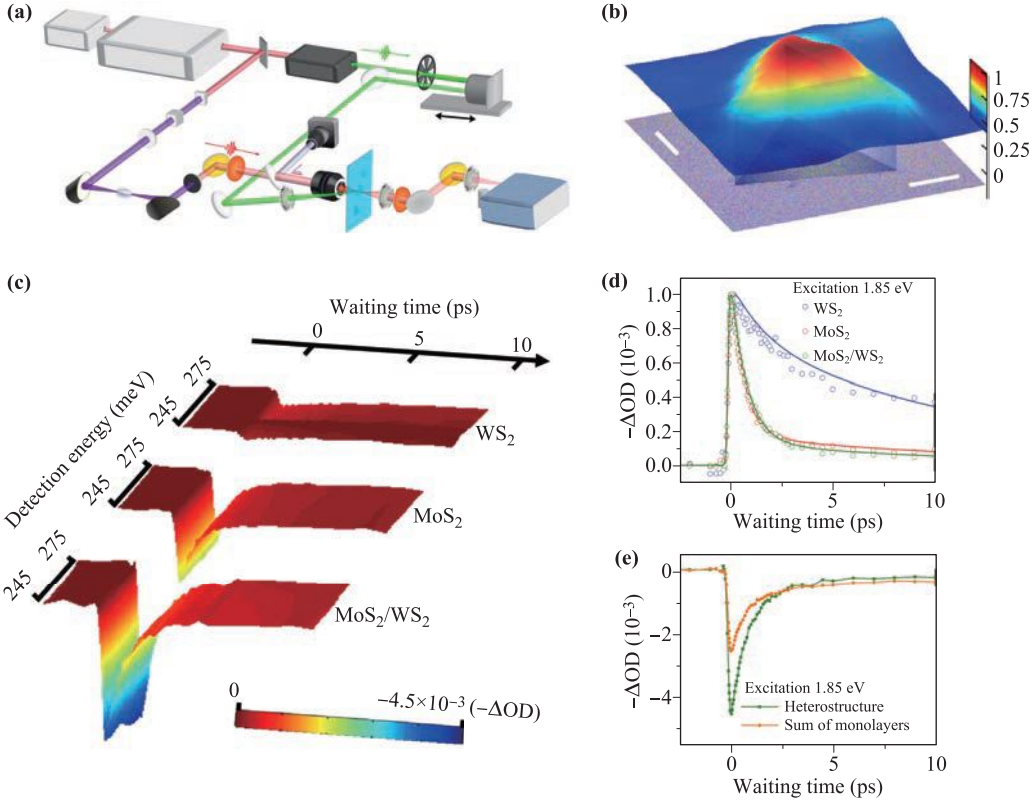

Fig. 10 The microspectroscopy measurements of ultrafast visible and IR region. **(a)** The schematic instructions of microspectroscopy measurements. **(b)** The transient absorption change of MoS_2/WS_2 heterostructure material. **(c)** The temporal evolution of the 670 nm excitation-induced absorption changes of WS_2, MoS_2 and the MoS_2/WS_2 heterostructure samples. **(d)** Normalized plots of temporal evolution. **(e)** The signal of the MoS_2/WS_2 heterostructure and the total of the WS_2 and MoS_2 monolayers. Reproduced from Ref. [227].

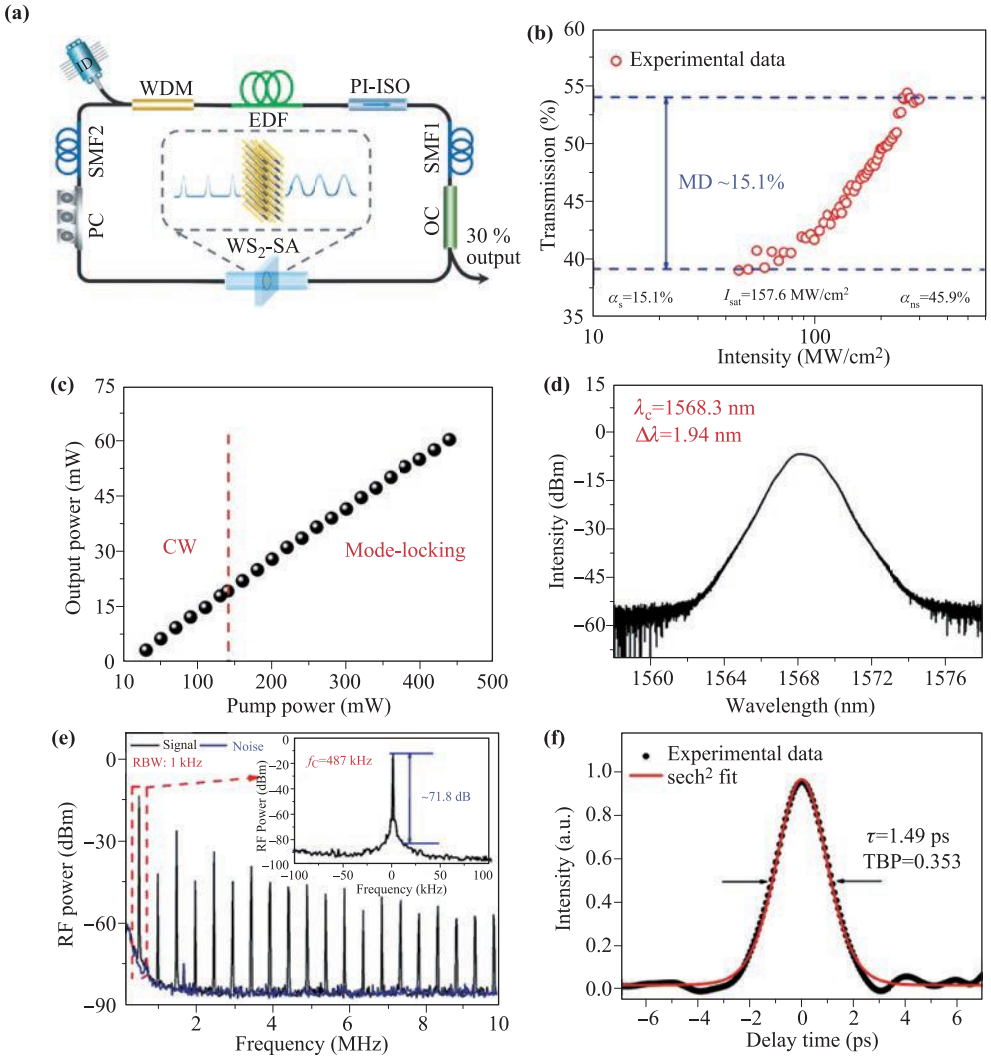

Fig. 11 **(a)** The experimental setup. **(b)** Nonlinear absorption curve. **(c)** The pump power versus laser output power.**(d)** Output spectrum with 3 dB bandwidth of 1.94 nm. **(e)** The RF spectrum. **(f)** Autocorrelation trace with a pulse duration of 1.49 ps after a sech^2 fitting. Reproduced from Ref. [228].

by employing mechanically exfoliated BP few-layer sheets and coated on the fiber ferrule. Their group employed an EDFL to obtain mode-locked pulse with the output pulse duration of 946 fs. But the main barrier that utilizes these strong absorption matearials to achieve high power output of the lasers is the low thermal damage threshold on account of the heating of the lasers. Lee *et al.* [16] searched a method that deposits BP onto side-polished fiber, where the saturable absorption takes place through the interaction between BP and evanescent interaction. This method can be employed to optimize the fiber laser operating at a higher power. In recent years, a microfiber-based BP quantum dot (QD) SA has been studied to display the strong nonlinear response at the wavelength of 1.56 μm, which indicates the latent value for the generation of ultrashort pulse [235, 236]. Figure 12(a) exhibits the configuration of an Er-doped fiber laser based on BPQD SA, and the output features of pulses are shown in Figs. 12(b)–(e). While no obvious change of central wavelength and spectral bandwidth can be observed, which indicates that the mode-locked state is very stable [235].

4.1.4 Pulsed fiber laser based on PbS SA

Recently, due to the advantages of small bandgap, high laser-induced damage threshold, excellent nonlinear absorption efficient and easy integration, there are some novel materials attracting researchers' attention, such as PbS nanoparticles and QDs, bismuthene, and Mxene. Hence, these novel materials are the promising optical devices in pulsed fiber lasers.

In 2018, Zhang's group and Yun's group both achieved mode-locked fiber laser based on the PbS nanoparticles and PbS QDs, respectively. As shown in Fig. 13, the

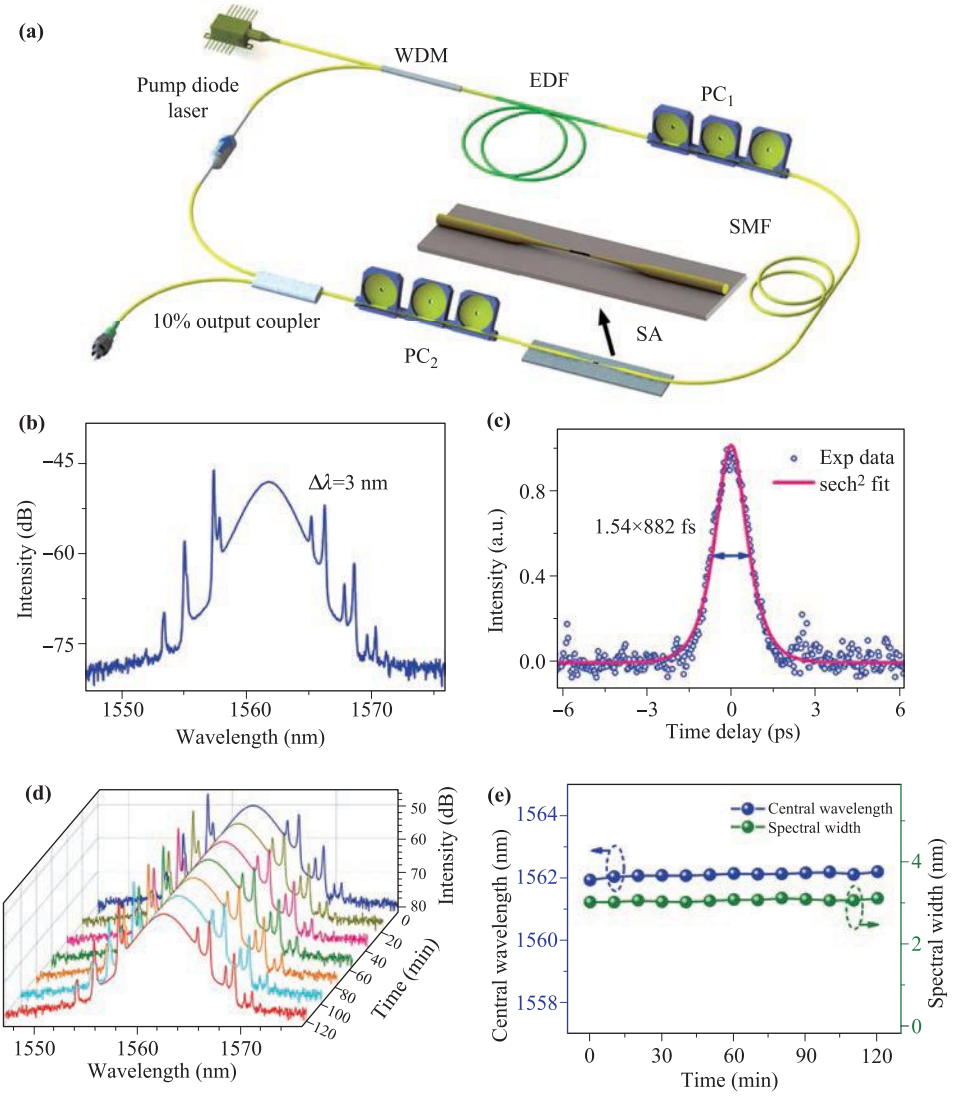

Fig. 12 **(a)** The schematic of fiber laser employing a microfiber-based BPQD. **(b)** Output optical spectrum. **(c)** Autocorrelation trace. **(d)** The optical spectra of the mode-locked operation at the time interval of 20 min. **(e)** The stability of the central wavelengths and the 3 dB bandwidth spectra. Reproduced from Ref [235].

mode-locked pulse with pulse width of 1.01 ps and spectrum width of 2.93 nm is obtained in an Er-doped fiber laser based on PbS NPs [237]. The experimental setup is shown in Fig. 13(a), and the results are shown in Figs. 13(b)–(e), respectively. In the same year, Yun *et al.* [238] realized a transform-limited soliton pulse with pulse duration of 559 fs and 3 dB bandwidth of 4.78 nm at the center wavelength of 1563 nm by incorporating PbS QDs into a fiber laser. The experimental setup is displayed in Fig. 14(a) and the results are shown in Figs. 14(b)–(e). Due to the nonlinear saturable absorption characteristics of PbS QDs, this material has practical applications in many fields, such as near-infrared (NIR) pulsed lasers and modulators.

Few-layered bismuthene, as a mono-elemental novel NBMs purely composed by the element of bismuth, has been theoretically predicted to possess an obviously enhanced stability and excellent optical responses. Few-layered bismuthene also has various significant properties, such as high carrier mobility, high stability, and excellent nonlinear optical transmission. Therefore, this material, as SA, has attracted tremendous interest in the application of fiber laser.

4.1.5 Pulsed fiber laser based on bismuthene SA

In 2018, Wang *et al.* [10] employed the few-layered bismuthene as the SA in the fiber laser. And the mode-locker is made by depositing the few-layered bismuthene on a microfiber. They successfully obtained the ultrashort pulse with duration of 621.5 fs, the spectrum bandwidth of 10.35 nm at the central wavelength of 1557.5 nm and funda-

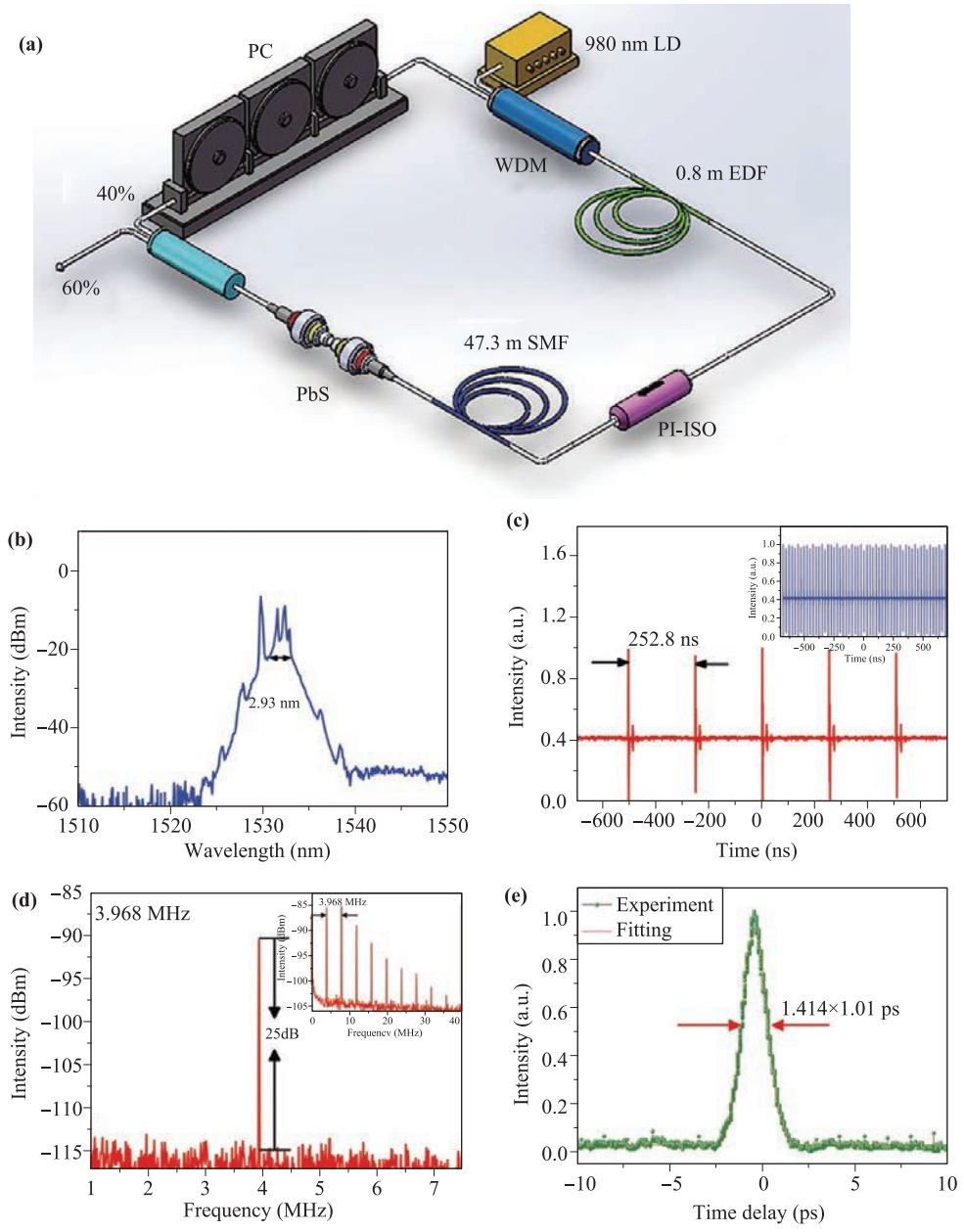

Fig. 13 **(a)** The setup of Er-doped fiber laser based on PbS NPs. **(b)** Output optical spectra. **(c)** Output pulse train at different range of 1400 ns and 4 μs. **(d)** RF spectrum. **(e)** Autocorrelation trace. Reproduced from Ref. [237].

mental repetition rate of 22.74 MHz, which can be seen in Figs. 15(a)–(d). And also they achieved the bound state soliton with the modulation period of 0.8 nm and pulse width of 525.5 fs in the proposed fiber laser at different

Table 1 The conclusion of fiber laser based on bismuthene SA.

Pulse duration	Spectrum bandwidth	Repetition rate	Central wavelength	Gain medium	Ref.
30.25 ps	2.72 nm	21.74 MHz	1034.4 nm	Yb	[9]
621.5 fs	10.35 nm	22.74 MHz	1557.5 nm	Er	[10]
652 fs	4.64 nm	8.83 MHz	1559.18 nm	Er	[99]
193 fs	14.4 nm	8.85 MHz	1561 nm	Er	[126]
1 ns	4.5 nm	16.7 MHz	2030 nm	Tm	[127]

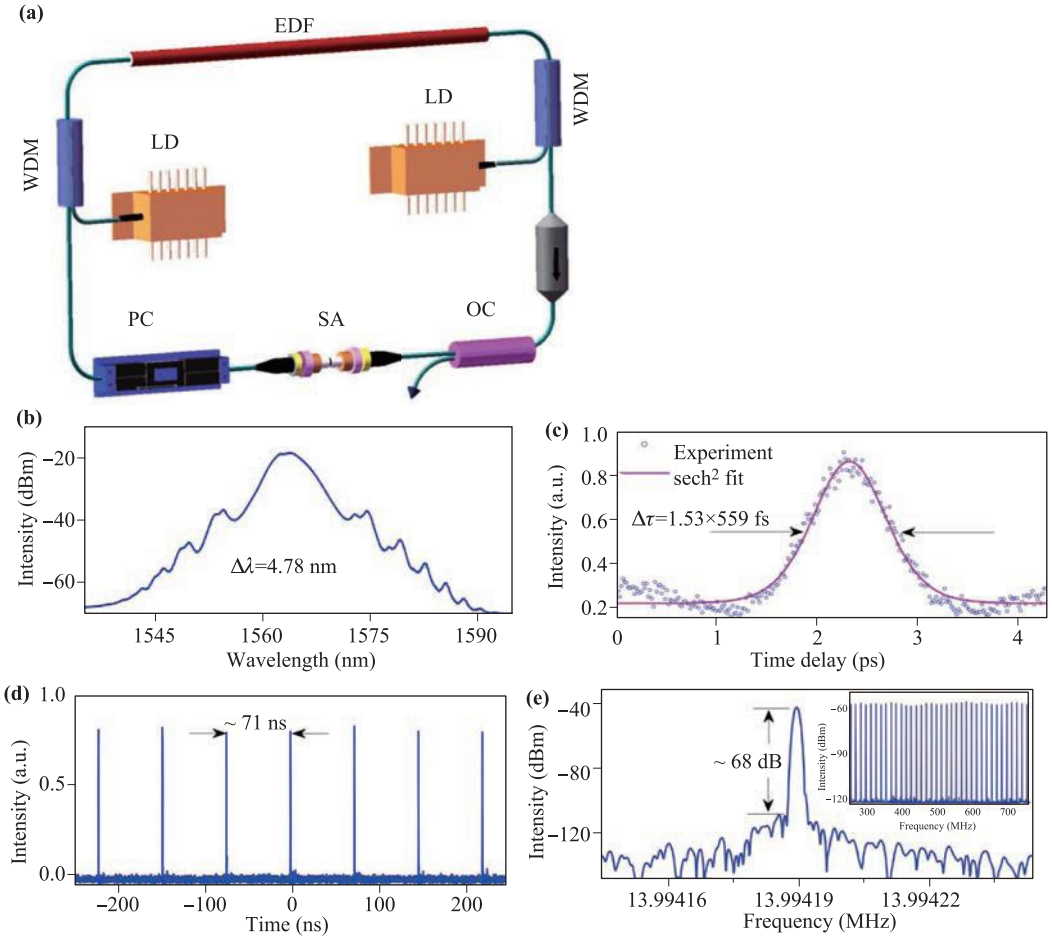

Fig. 14 **(a)** The schematic of PbS QD mode-locked fiber laser. **(b)** Output spectrum. **(c)** Pulse train. **(d)** The pulse train. **(e)** Radio frequency spectrum. Reproduced from Ref. [238].

pump power and polarization state, which can be seen in Figs. 15(e) and (f). Chai *et al.* [9] studied the Yb-doped ring fiber laser using bismuthene for the generation of ultrashort pulse based on evanescent field. And they successfully achieved the conventional solitons with duration of 30.25 ps at the wavelength of 1034.4 nm. The characteristics of output are shown in Figs. 16(a)–(d), respectively. In the same year, Yang *et al.* [127] achieved the Tm-doped fiber laser based on a 17-layer thickness bismuthene. The schematic diagram is exhibited in Fig. 17(a). And the output pulse with duration of 1 nm and 3 dB spectrum bandwidth of 4.5 nm was obtained, as shown in Figs. 17(b) and (c), accordingly.

In recent years, many studies based on bismuthene [9, 10, 99, 127, 239–241] have emerged. And the researches about the fiber laser were concluded in Table 1. Hence, we demonstrate that the study of bismuthene can be regarded as a novel direction of up-and-coming SA materials with high stability and excellent nonlinear optical characterizations. In addition to the materials mentioned above, the variety of 2D materials has constantly been enriched in recent years, such as TIs [242–244], MXene [245–247], antimonene [248], and perovskite [249], which exhibit sundry properties, therefore they are the promising candidates for the applications of ultrafast photonics.

4.1.6 The various pulse laser technologies

Different from the semiconductor saturable absorber mirrors (SESAMs) that have the limited saturable absorption bandwidth, the NBMs have wide saturable absorption bandwidth. And the fabrication cost of SESAMs is much higher than that of NBMs. The SESAMs operate in reflection while the NBMs integrate into solid state or fiber lasers in different ways. As for solid state laser, the simplest way to manufacture SA is to deposit the NBMs dispersion on a flat substrate, such as mirrors or the quartz glass plates, and in this way, it makes the SA operates in transmission or reflection. As for fiber lasers, various methods have been stated for the NBMs SA integrated in the system. As shown in Fig. 18 [222, 250–253], the SA can be fabricated by deposition of the NBMs dispersion on the surface of fiber connector, or on side-polished fiber

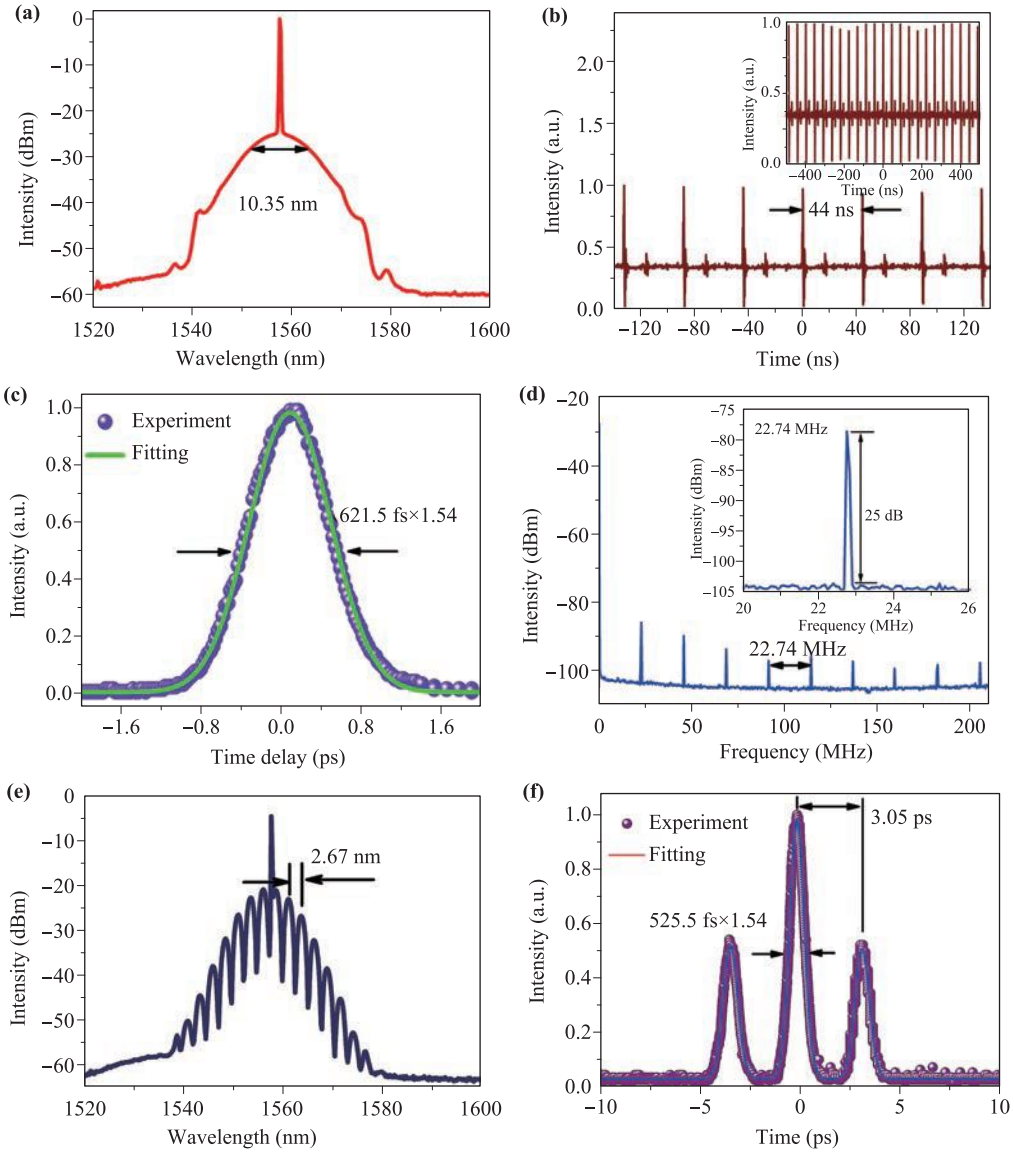

Fig. 15 **(a)** Output spectrum; **(b)** Out pulse train. **(c)** The autocorrelation trace with pulse duration of 621.5 fs. **(d)** The RF spectrum. **(e)** Output spectrum of bound state solitons. **(f)** Autocorrelation trace of bound state solitons. Reproduced from Ref. [10].

or tapered fiber.

4.2 Optical modulation based on NBMs

4.2.1 The typical methods of optical modulation based on NBMs

The NBMs' optical response to the incident light can be characterized through dielectric constant or conductivity or refractive index, and it can be modified by the external field such as optical, magnetic, or electric field, and temperature or pressure. Hence, the light that propagates through the certain NBMs can be modulated by another beam light (called as all-optical modulation) or the electric field (called as electro-optical modulation). The typical methods of optical modulation based on NBMs are divided into three types through the different applied external fields, such as thermal heating, electrical gating, and optical excitation, as exhibited in Fig. 19 [254]. And the optical excitation and the external electrical gating adjust the complex refractive index and the carrier density of the NBMs, which can be applied in the generation of the amplitude modulation and phase modulation. The thermal heating produced in the NBMs, whether electrical-induced or the optical-induced, is spread to the transparent substrate or waveguide, which elevates the temperature and then altering the real part of the refractive index, which is generally utilized for the phase modulation.

As for monolayer graphene, the Fermi energy of material is apparently varied to modify the optical transition

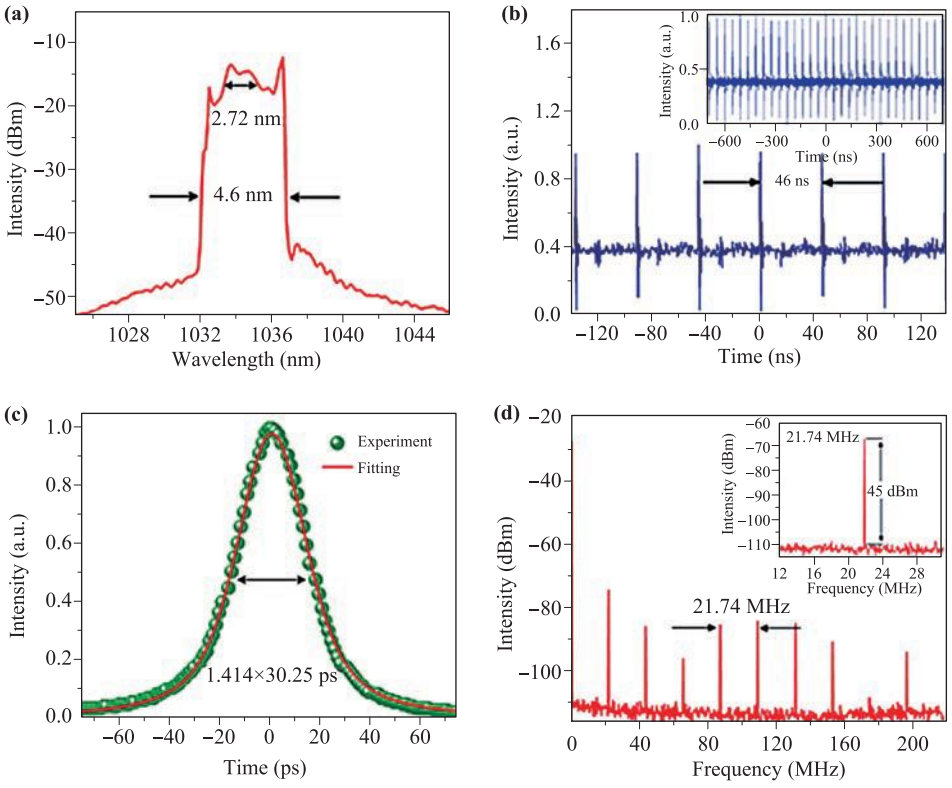

Fig. 16 **(a)** The output optical spectrum. **(b)** The output pulse train. **(c)** Autocorrelation trace. **(d)** The RF spectrum. Reproduced from Ref. [9].

of interband when inflicting the bias electric field. Figure 20(a) shows the gate voltage dependent reflection rate of graphene on a silicon substrate, and the inset figure demonstrates the interband transition of the monolayer graphene. While the all-optic method for the optical modulation based on NBMs is used by applying the ultrashort pulses to regulate the propagation of the signal, providing the ultrafast response based on the optical nonlinear effects [255]. Due to the relatively low density of state and zero bandgap of graphene, optical excitation generates the nonequilibrium carriers in the valence band and conduction band, which results in the extremely strong saturable

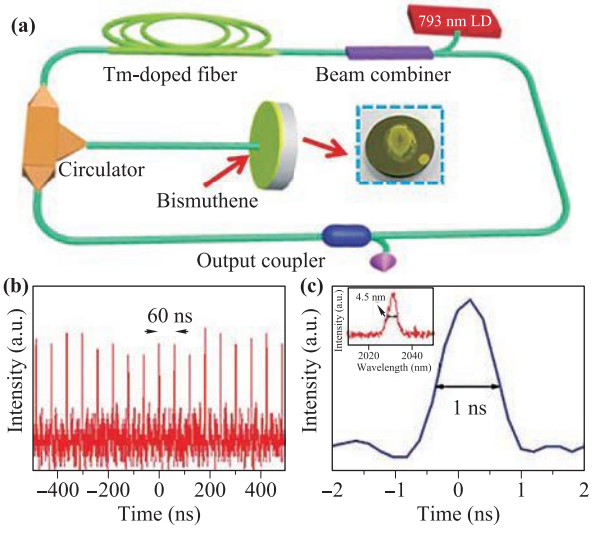

Fig. 17 **(a)** Experimental setup. **(b)** Output pulse train. **(c)** Output pulse, and the inset is the output spectrum. Reproduced from Ref. [127].

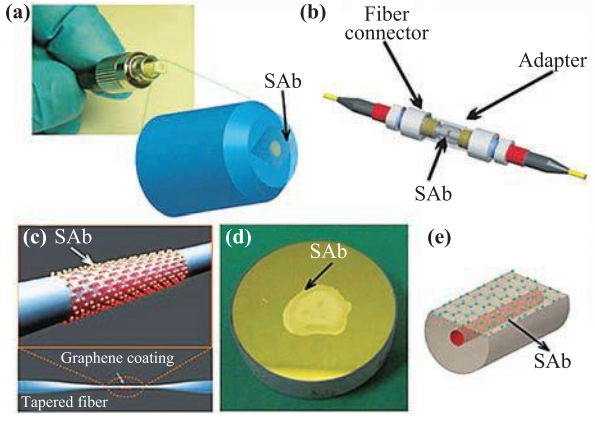

Fig. 18 The schematic devices of NBMs based on SA. **(a)** The film coated on pigtail of fiber. **(b)** Materials inset between two fiber connectors. **(c)** Dispersion of material deposited on microfiber or tapered fiber. **(d)** Material coated on the mirror. **(e)** Material deposited on D-shaped fiber. Reproduced from Refs. [222, 250–253].

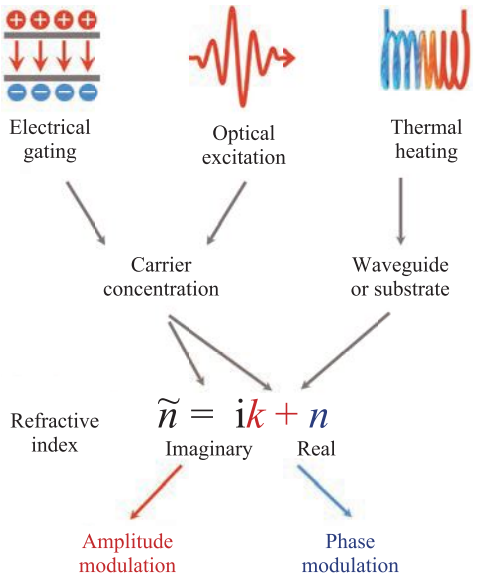

Fig. 19 The typical methods of optical modulation based on NBMs. Reproduced from Ref. [254].

absorption with the ultrashort response time [256]. And it can be widely applied in mode-locked fiber lasers and the optical modulators. Figure 20(b) [257] shows the theoretical and experimental results of the nonlinear refractive index based on graphene. Due to the high thermal conductivity of the graphene at the room temperature, the NBMs diffuse the heat to their surrounding materials, which could be used as the heat generator and conductor [258, 259].

4.2.2 The typical systems of optical modulation based on NBMs

The typical systems of optical modulation include free space optical modulation [255, 256], fiber-based optical modulation [262–265], and chip integrated optical modulation. There are many different structures of the optical modulation listed follows. Sensale-Rodriguez *et al.* [266] put forward a kind of wideband graphene terahertz (THz) modulator and achieved by the intraband transition in 2012, as shown in Fig. 21(a). As shown in Fig. 21(b), a gating voltage is used between a back ring-shaped contact on the substrate and a top contact on monolayer graphene to adjust the Fermi level of graphene. Figure 21(c) exhibits the modulator composes of the accumulated graphene pairs with capacitive-coupled 2D hole gases (2DHG) in the valence band and 2D electron gases (2DEG) in the conduction band, so that it can surmount potentially limited modulation by using a single-layer graphene [267]. At zero bias ($V_g = 0$ V), it causes the minimum loss of insertion or the attenuation of signal when the Fermi level is at the Dirac point of all layers of graphene. When the bias voltage is applied, 2DEGs are in one of the graphene layers linked to the negative electrode and 2DHGs are in another of graphene layers linked to the positive electrode, which leads to the near-zero terahertz transmission.

In 2014, Wen *et al.* [268] achieved a maximum modulation depth of 94% based on an all-optical structure where the 1550 nm incident light acts as the incident light to excite carrier in graphene and cause the third-order nonlinear effect, as exhibited in Fig. 22(a). And Fig. 22(b) shows the time domain THz transmittance of graphene on germanium (GOG) represented by dashed curves and germanium (Ge) represented by the solid curves without and with the photo-doping, respectively, and the inset figure is the peak–peak amplitude with the variation of pump power. The experimental configuration for the measurements of modulation features is shown in Fig. 22(c).

In free space modulation configurations in which the pump light passes through and interacts with the material merely once, the interaction between light and matter is generally not robust enough for the employments that required large modulation depth (MD). The LBM is integrated with a variety of the resonant structures in order

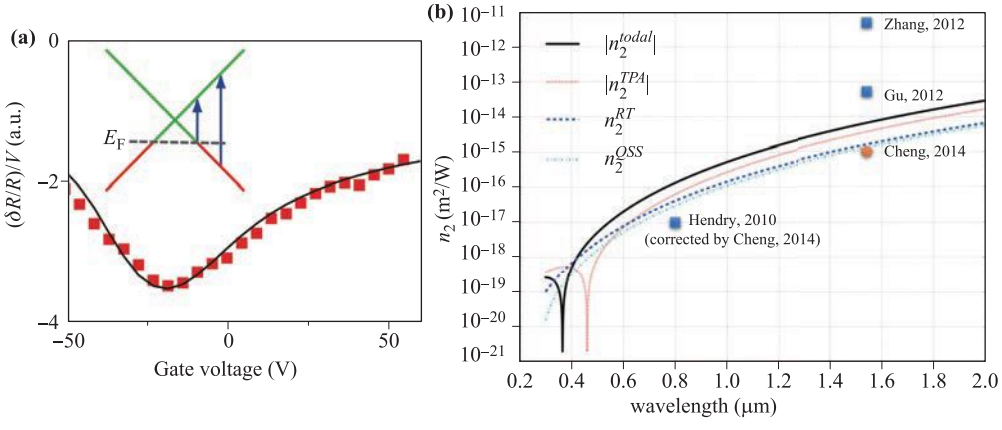

Fig. 20 **(a)** The gate voltage dependent reflection rate of graphene on a silicon substrate. **(b)** The theoretical values represented in the green point and purple line and the experimental values represented in color points except for the green of the graphene refractive index. (a) Reproduced from Ref. [253], (b) Reproduced from Ref. [257].

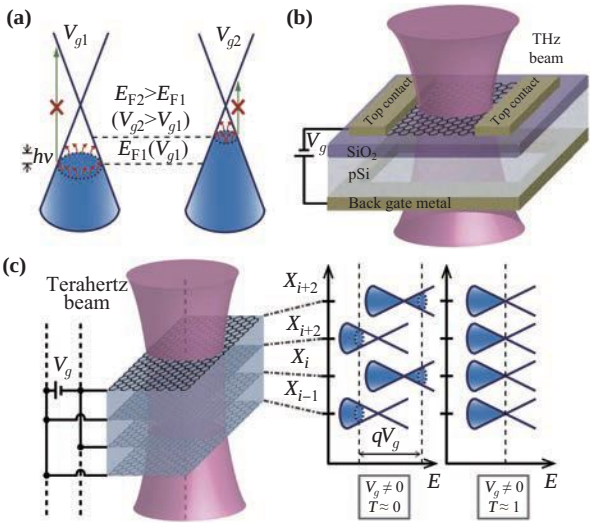

Fig. 21 The operating principle and modulator structures. **(a)** Diagram of intraband transition enabled THz modulators. **(b)** The diagram of the graphene THz modulator. **(c)** THz modulator composed of accumulated graphene pairs with capacitive-coupled 2DEG in the conduction band and 2DHG in the valence band. (a) Reproduced from Ref. [266], (b, c) Reproduced from Ref. [267].

to boost the interaction between the light and material, and the structures have many types, such as Fano resonant structures shown in Figs. 23(a) and (b). Figures 23(c) and (d) show the photonic crystal cavities, metasurfaces structures, respectively. And the metal plasmonic antenna arrays structures. All these structures are designed to process a Fano or plasmonic resonance at THz or MIR wavelength. Figure 23(a) shows a diagram of adjustable plasmonic equipment possessing 3 dB cutoff frequency of 30 MHz that will be further enhanced to the range of gigahertz (GHz) [269]. It convinces that the structures of hybrid metal graphene are excellent factors for the production of ultrahigh speed electrical-controllable optoelectronic and optical facilities. Figure 23(b) uses the electrically adjustable interband transitions in graphene to charge the intensity of the plasmonic resonance [270]. Figure 23(c) shows an all-optical structure [271]. Due to the possibility of flexibly controlling its complex refractive index, when a pump power is reduced to tens of milliwatts, it will lead to a resonance wavelength shift of 3.5 nm. And these graphene integrated metamaterials exhibit the possibility of modifying both phase and intensity of the light in the interaction between light and materials. As shown in Fig. 23(d) [272], Bumki *et al.* demonstrated that the linear modulation of THz wave and the gating induced sustaining switching can be obtained in a metamaterial, in which the integration of a thin and gated graphene layer is successfully achieved. A THz pump wave is modulated by the intensity change of 47% and phase rotation

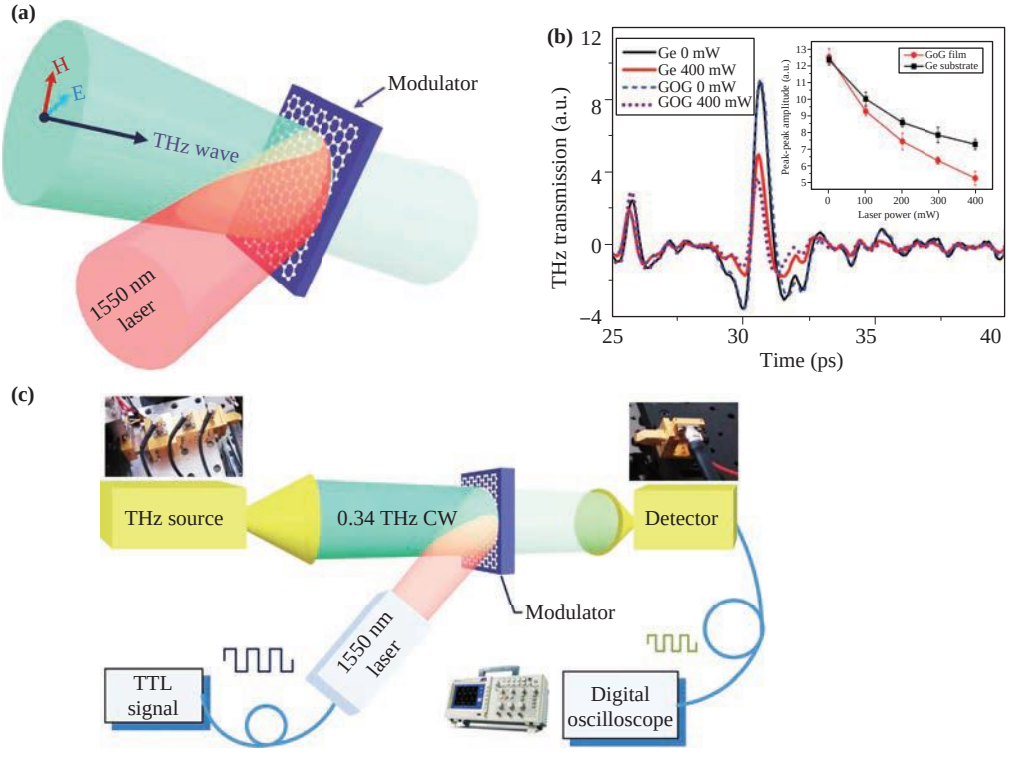

Fig. 22 **(a)** The structure of the all-optical spatial THz modulator. **(b)** The time domain spectra and the inset figure shows amplitude of the main THz pulse with the increasing of pump power. **(c)** The experimental configuration applied in the measurement of modulation. Reproduced from Ref. [268].

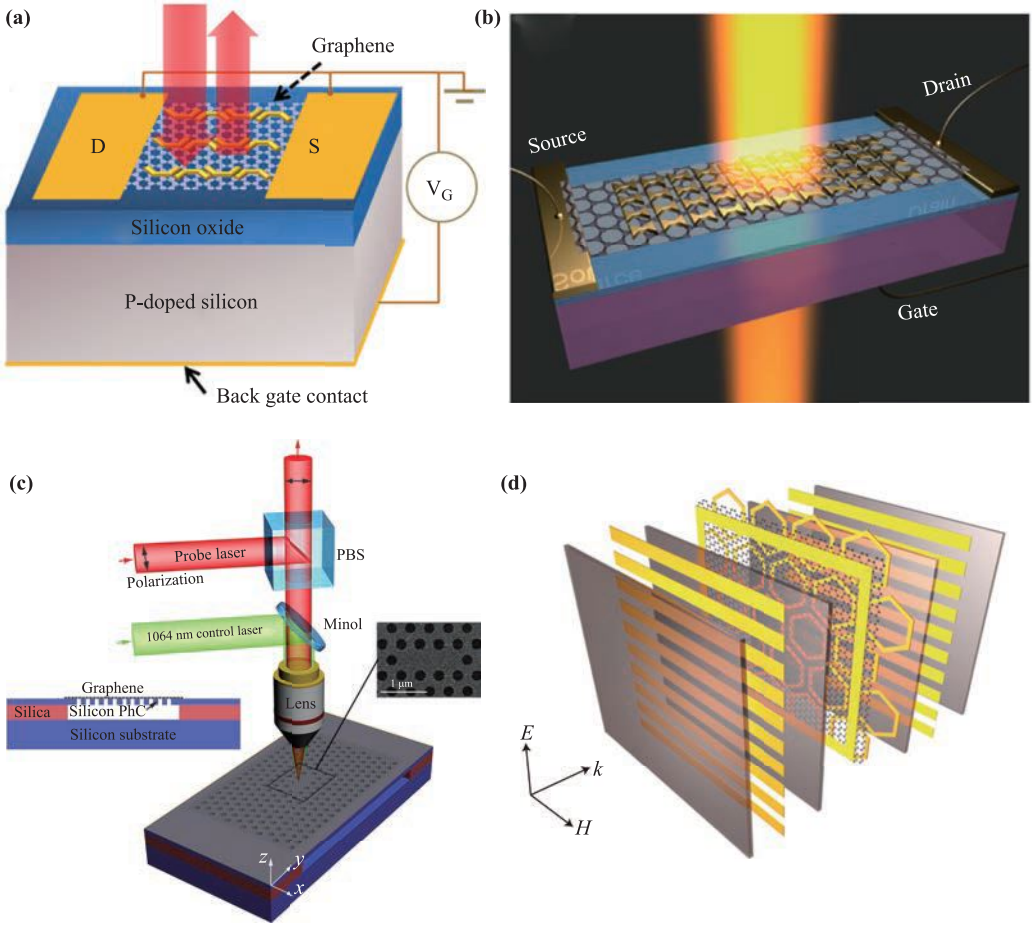

Fig. 23 **(a)** The setup of the adjustable plasmonic facility. **(b)** Graphene-bowtie plasmonic structure for voltage controlled optical transmission measurements. **(c)** A cross-polarized reflectivity measurement on the hybrid structure of grapheme. **(d)** The diagram of gate-controlled active graphene metamaterial. (a) Reproduced from Ref. [269], (b) Reproduced from Ref. [270], (c) Reproduced from Ref. [271], (d) Reproduced from Ref. [272].

of 32.2° at the same time, offering the new opportunities for the employment in polarization rotators, thin optical modulators, and nonreciprocal devices.

With the booming studies of these novel materials, including graphene, TMDCs, BP, h-BN, TIs, semimetal materials and various narrow-bandgap semiconductors, they have already been widely researched for different applications including photodetector [273–275], biomedical [276–280], sensors [281–283], battery [284, 285], and so on. These novel materials show many merits, such as great optical and electric properties, and the prefect nonlinear optical response exhibited with the strong or reverse saturable absorption. These narrow-bandgap emerging materials exhibit excellent elements for the application in the fields of ultrafast photonics and nonlinear optics due to their simple accessibility employing the methods of mechanical exfoliation or liquid phase exfoliation and easy integration of devices. SAs prepared by these various NBMs have obvious differences in the saturable intensity, modulation depth and relaxation time. All these differences rely on the intrinsic and extrinsic characteristics of materials and the fabrication procedures.

According to the above analysis, first of all, from the material band gap, the graphene band gap ranging from 0 to 0.25 eV. MoS_2 has a special energy band structure different from graphene, that is, the indirect band gap. Its forbidden band width is 1.29 eV, and the forbidden band width will increase as the number of molybdenum disulfide layers decreases. The band gap of the monolithic MoS_2 is 1.8 eV, and the band structure also becomes a direct band gap at this time. Therefore, the monolithic MoS_2 is not only a semiconductor material, but also has photocatalytic activity. The band gap of WS_2 is 2 eV. The band gap of black phosphorous (BP) can be adjusted from 0.3 eV (multilayer) to 2 eV (single layer), and it is also a material with adjustable band gap. The band gap of PbS is 0.4 eV, and the band gap of Bi is about 0.14 eV. It can be seen that the band gaps of the above materials are very small, which is very suitable for mode-locked pulse lasers. Furthermore, graphene can be used as a saturable absorber to generate pulses ranging from visible light to infrared in pulsed lasers due to its ultra-fast recovery time, ultra-wide nonlinear

optical response bandwidth, and super-saturated absorption. Because the exit of edge states and defect states helps MoS_2 SA work in near-infrared and MIR, it is possible to describe fiber lasers with wavelengths far exceeding the exciton absorption wavelength. In solid-state lasers based on volumetric cavity, due to the highly unsaturated loss of MoS_2 SAs, mode-locked pulses still cannot be generated, but mode-locked pulses can be obtained in fiber lasers. However, the Q-switch produced in the solid-state laser can achieve higher output power and lower repetition rate, which shows that this material is more suitable for realizing the function similar to Q-switch in laser. The narrow band gap and adjustable band gap of black phosphorous (BP) make it very suitable for ultrafast photonics. Therefore, when studying ultrashort pulse fiber lasers, we can find that materials with a narrower band gap are more advantageous in achieving mode-locking performance, because the smaller the band gap is, the larger the range of light absorption will be, and the wider the range of applications for ultrafast photonics.

5 Conclusions and outlook

These novel and flexible NBMs have vast applications in the fields of mode-locker, Q-switcher, modulator, detector, transistor and optical limiter. They have realized short pulses generation based on mode locking and Q-switching both in solid-state and fiber laser. Up to now, the optical modulation based on NBMs has acquired great achievements in many aspects, and covering from theoretical optimal design and analysis, the preparation of the materials, the integration methods between materials and devices to the structures of modulator. These results indicate the excellent opportunities of employing NBMs for many types of optical modulation, such as free space optical modulation, fiber-based amplitude modulation, and fiber-based phase modulation.

The materials discussed in this article are all narrow band gap materials with very excellent nonlinear optical properties. However, each material also has its own morphology, such as light absorption intensity and element composition. These factors all directly or indirectly affect its scope of application. These characteristics of the material can be observed through its characterization results. The narrow band gap material studied in this article also has excellent light absorption properties, and the smaller the band gap the material has, the larger the absorption spectrum and the wider the application range of ultrafast photonics. Therefore, materials with a narrow band gap are more suitable for infrared ultrafast photonics applications.

Nevertheless, the studies are focused on the characteristics of these NBMs, while as for the practical applications are still a vast challenge. The biggest challenge in commercial SAs exists in long term stability of these NBMs, particular under the operation of high pump power. But the intelligent structures of laser partly figure out this problem. For a more thorough solution, we can add organic modification materials on the surface of the material. The SAs made of phosphorous, chalcogenides or the polymers like polyvinyl alcohol (PVA) and polymethyl methacrylate (PMMA) should avoid the thermal damage and oxidization. Thermal damage will affect the thermal shock resistance of the material, and oxidation will change some properties of the material. In order to prevent thermal damage and oxidation of materials, we need to passivate the materials. Although BP as a novel family member of NBMs has superior photoelectric characteristics, the low environmental stability is one of the biggest adverse factors restricting its practical application, and it is also an important research topic in the field of these NBMs. Therefore, not all narrow band gap materials are suitable for fiber lasers. When we use a material, we should make full investigation to determine whether the material is suitable for the desired effect according to its characteristics.

It is one of the most significant research directions to study and apply the nonlinear optical features of these novel NBMs as SA in laser pulse generation and modulation. This field has obtained fruitful achievements, but there are still some problems to be solved at the same time, including how to enhance the laser-induced damage threshold of NBMs (especially TMDCs, TIs, and BP) and environmental stability in the process of application, and integration with fiber optic devices more effectively in the applications of fiber laser. These are all topics that need further studies in near future.

Acknowledgements This research was supported by the National Natural Science Foundation of China (Grant Nos. 61605106, 61875138, 61435010, and 6181101252); the International Science & Technology Cooperation and Exchanges Project of Shaanxi (No. 2020KW-005); Funded projects for the Academic Leader and Academic Backbones, Shaanxi Normal University (No. 18QNGG006); Starting Grants of Shaanxi Normal University (Grant Nos. 1112010209 and 1110010717); Fundamental Research Funds For the Central Universities (No. GK201802006); and the Open Research Fund of State Key Laboratory of Transient Optics and Photonics, Chinese Academy of Sciences (No. SKLST201809).

References

1. K. S. Novoselov, A. K. Geim, S. V. Morozov, D. Jiang, Y. Zhang, S. V. Dubonos, I. V. Grigorieva, and A. A. Firsov, Electric field effect in atomically thin carbon films, *Science* 306(5696), 666 (2004)
2. R. R. Nair, P. Blake, A. N. Grigorenko, K. S. Novoselov, T. J. Booth, T. Stauber, N. M. Peres, and A. K. Geim, Fine structure constant defines visual transparency of graphene, *Science* 320(5881), 1308 (2008)

3. Z. H. Ni, H. M. Wang, J. Kasim, H. M. Fan, T. Yu, Y. H. Wu, Y. P. Feng, and Z. X. Shen, Graphene thickness determination using reflection and contrast spectroscopy, *Nano Lett.* 7(9), 2758 (2007)
4. X. Du, I. Skachko, A. Barker, and E. Y. Andrei, Approaching ballistic transport in suspended graphene, *Nat. Nanotechnol.* 3(8), 491 (2008)
5. K. S. Kim, Y. Zhao, H. Jang, S. Y. Lee, J. M. Kim, K. S. Kim, J. H. Ahn, P. Kim, J. Y. Choi, and B. H. Hong, Large-scale pattern growth of graphene films for stretchable transparent electrodes, *Nature* 457(7230), 706 (2009)
6. A. Pospischil and T. Mueller, Optoelectronic devices based on atomically thin transition metal dichalcogenides, *Appl. Sci. (Basel)* 6(3), 78 (2016)
7. P. F. Chen, N. Li, X. Z. Chen, W.-J. Ong, and X. J. Zhao, The rising star of two-dimensional black phosphorus beyond graphene: Synthesis, properties and electronic applications, *2D Materials* 5, 014002 (2017)
8. A. Zhuang, J. J. Li, Y. C. Wang, X. Wen, Y. Lin, B. Xiang, X. P. Wang, and J. Zeng, Screw-dislocation-driven bidirectional spiral growth of Bi_2Se_3 nanoplates, *Angew. Chem. Int. Ed.* 53(25), 6425 (2014)
9. T. Chai, X. Li, T. Feng, P. Guo, Y. Song, Y. Chen, and H. Zhang, Few-layer bismuthene for ultrashort pulse generation in a dissipative system based on an evanescent field, *Nanoscale* 10(37), 17617 (2018)
10. C. Wang, L. Wang, X. Li, W. Luo, T. Feng, Y. Zhang, P. Guo, and Y. Ge, Few-layer bismuthene for femtosecond soliton molecules generation in Er-doped fiber laser, *Nanotechnology* 30(2), 025204 (2019)
11. M. Chernysheva, A. Rozhin, Y. Fedotov, C. Mou, R. Arif, S. M. Kobtsev, E. M. Dianov, S. K. Turitsyn, Carbon nanotubes for ultrafast fiber lasers, *Nanophotonics* 6(1), 1 (2016)
12. Q. L. Bao, H. Zhang, Y. Wang, Z. H. Ni, Y. L. Yan, Z. X. Shen, K. P. Loh, and D. Y. Tang, Atomic-layer graphene as a saturable absorber for ultrafast pulsed lasers, *Adv. Funct. Mater.* 19(19), 3077 (2009)
13. I. H. Baek, K. J. Ahn, B. J. Kang, S. Bae, B. H. Hong, D. I. Yeom, K. Lee, Y. U. Jeong, and F. Rotermund, Terahertz transmission and sheet conductivity of randomly stacked multi-layer graphene, *Appl. Phys. Lett.* 102(19), 191109 (2013)
14. S. Davide Di Dio Cafiso, E. Ugolotti, A. Schmidt, V. Petrov, U. Griebner, A. Agnesi, W. B. Cho, B. H. Jung, F. Rotermund, S. Bae, B. H. Hong, G. Reali, and F. Pirzio, Sub-100-fs Cr:YAG laser mode-locked by monolayer graphene saturable absorber, *Opt. Lett.* 38(10), 1745 (2013)
15. E. Ugolotti, A. Schmidt, V. Petrov, J. Wan Kim, D. I. Yeom, F. Rotermund, S. Bae, B. Hee Hong, A. Agnesi, C. Fiebig, G. Erbert, X. Mateos, M. Aguiló, F. Diaz, and U. Griebner, Graphene mode-locked femtosecond Yb:KLuW laser, *Appl. Phys. Lett.* 101(16), 161112 (2012)
16. K. F. Mak, J. Shan, and T. F. Heinz, Seeing many-body effects in single- and few-layer graphene: Observation of two-dimensional saddle-point excitons, *Phys. Rev. Lett.* 106(4), 046401 (2011)
17. G. Demetriou, H. T. Bookey, F. Biancalana, E. Abraham, Y. Wang, W. Ji, and A. K. Kar, Nonlinear optical properties of multilayer graphene in the infrared, *Opt. Express* 24(12), 13033 (2016)
18. T. Winzer, R. Ciesielski, M. Handloser, A. Comin, A. Hartschuh, and E. Malic, Microscopic view on the ultrafast photoluminescence from photoexcited graphene, *Nano Lett.* 15(2), 1141 (2015)
19. K. J. Tielrooij, J. C. W. Song, S. A. Jensen, A. Centeno, A. Pesquera, A. Z. Elorza, M. Bonn, L. S. Levitov, and F. H. L. Koppens, Photoexcitation cascade and multiple hot-carrier generation in grapheme, *Nat. Phys.* 9, 248 (2013)
20. M. Breusing, C. Ropers, and T. Elsaesser, Ultrafast carrier dynamics in graphite, *Phys. Rev. Lett.* 102(8), 086809 (2009)
21. M. Breusing, S. Kuehn, T. Winzer, E. Malić, F. Milde, N. Severin, J. P. Rabe, C. Ropers, A. Knorr, and T. Elsaesser, Ultrafast nonequilibrium carrier dynamics in a single graphene layer, *Phys. Rev. B* 83(15), 153410(2011)
22. P. A. George, J. Strait, J. Dawlaty, S. Shivaraman, M. Chandrashekhar, F. Rana, and M. G. Spencer, Ultrafast optical-pump terahertz-probe spectroscopy of the carrier relaxation and recombination dynamics in epitaxial graphene, *Nano Lett.* 8(12), 4248 (2008)
23. C. H. Lui, K. F. Mak, J. Shan, and T. F. Heinz, Ultrafast photoluminescence from graphene, *Phys. Rev. Lett.* 105(12), 127404 (2010)
24. L. Miao, Y. Jiang, S. Lu, B. Shi, C. Zhao, H. Zhang, and S. Wen, Broadband ultrafast nonlinear optical response of few-layers graphene: Toward the mid-infrared regime, *Photon. Res.* 3(5), 214 (2015)
25. Y. Wang, H. Mu, X. Li, J. Yuan, J. Chen, S. Xiao, Q. Bao, Y. Gao, and J. He, Observation of large nonlinear responses in a graphene-Bi_2Te_3 heterostructure at a telecommunication wavelength, *Appl. Phys. Lett.* 108(22), 221901 (2016)
26. Q. L. Bao, H. Zhang, Y. Wang, Z. H. Ni, Y. L. Yan, Z. X. Shen, K. P. Loh, and D. Y. Tang, Atomic-layer graphene as a saturable absorber for ultrafast pulsed lasers, *Adv. Funct. Mater.* 19(19), 3077 (2009)
27. S. R. Bongu, P. B. Bisht, R. C. K. Namboodiri, P. Nayak, S. Ramaprabhu, T. J. Kelly, C. Fallon, and J. T. Costello, Influence of localized surface plasmons on Pauli blocking and optical limiting in graphene under femtosecond pumping, *J. Appl. Phys.* 116(7), 073101 (2014)
28. J. J. Dean and H. M. V. Driel, Graphene and few-layer graphite probed by second-harmonic generation: Theory and experiment, *Phys. Rev. B* 82(12), 3893(2010)
29. M. Zhang, G. Li, and L. Li, Graphene nanoribbons generate a strong third-order nonlinear optical response upon intercalating hexagonal boron nitride, *J. Mater. Chem. C* 2(8), 1482 (2014)
30. Q. H. Wang, K. Kalantar-Zadeh, A. Kis, J. N. Coleman, and M. S. Strano, Electronics and optoelectronics of two-dimensional transition metal dichalcogenides, *Nat. Nanotechnol.* 7(11), 699 (2012)

31. H. Tian, M. L. Chin, S. Najmaei, Q. Guo, F. Xia, H. Wang, and M. Dubey, Optoelectronic devices based on two-dimensional transition metal dichalcogenides, *Nano Res.* 9(6), 1543 (2016)
32. J. Liu, H. Cao, B. Jiang, Y. Xue, and L. Fu, Newborn 2D materials for flexible energy conversion and storage, *Science China Mater.* 59(6), 459 (2016)
33. K. F. Mak and J. Shan, Photonics and optoelectronics of 2D semiconductor transition metal dichalcogenides, *Nat. Photonics* 10(4), 216 (2016)
34. R. I. Woodward and Kelleher, Saturable absorbers for fibre lasers, *Appl. Sci. (Basel)* 5(4), 1440 (2015)
35. T. Shishidou, A. J. Freeman, and R. Asahi, Effect of GGA on the half-metallicity of the itinerant ferromagnet, *Phys. Rev. B* 64(18), 180401(2001)
36. K. Takada, H. Sakurai, E. Takayama-Muromachi, E Izumi, R. Dilanian, and T. Sasaki, Superconductivity in two-dimensional CoO_2 layers, *Nature* 422(6927), 53 (2003)
37. J. T. Jang, S. Jeong, J. W. Seo, M. C. Kim, E. Sim, Y. Oh, S. Nam, B. Park, and J. Cheon, Ultrathin zirconium disulfide nanodiscs, *J. Am. Chem. Soc.* 133(20), 7636 (2011)
38. J. W. Seo, Y. W. Jun, S. W. Park, H. Nah, T. Moon, B. Park, J. G. Kim, Y. J. Kim, and J. Cheon, Two-dimensional nanosheet crystals, *Angew. Chem. Int. Ed. Engl.* 46(46), 8828 (2007)
39. M. R. Gao, X. Cao, Q. Gao, Y. F. Xu, Y. R. Zheng, J. Jiang, and S. H. Yu, Nitrogen-doped graphene supported $CoSe_2$ nanobelt composite catalyst for efficient water oxidation, *ACS Nano* 8(4), 3970 (2014)
40. C. Altavilla, M. Sarno, and P. Ciambelli, A novel wet chemistry approach for the synthesis of hybrid 2D free-floating single or multilayer nanosheets of MS_2@oleylamine (M=Mo, W), *Chem. Mater.* 23(17), 3879 (2011)
41. S. Jeong, D. Yoo, J. T. Jang, M. Kim, and J. Cheon, Well-defined colloidal 2-D layered transition-metal chalcogenide nanocrystals via generalized synthetic protocols, *J. Am. Chem. Soc.* 134(44), 18233 (2012)
42. B. Radisavljevic, A. Radenovic, J. Brivio, V. Giacometti, and A. Kis, Single-layer MoS_2 transistors, *Nat. Nanotechnol.* 6(3), 147 (2011)
43. B. W. Baugher, H. O. Churchill, Y. Yang, and P. Jarillo-Herrero, Intrinsic electronic transport properties of high-quality monolayer and bilayer MoS_2, *Nano Lett.* 13(9), 4212 (2013)
44. D. Lembke and A. Kis, Breakdown of high-performance monolayer MoS_2 transistors, *ACS Nano* 6(11), 10070 (2012)
45. G. Eda and S. A. Maier, Two-dimensional crystals: Managing light for optoelectronics, *ACS Nano* 7(7), 5660 (2013)
46. L. Yang, K. Majumdar, H. Liu, Y. Du, H. Wu, M. Hatzistergos, P. Y. Hung, R. Tieckelmann, W. Tsai, C. Hobbs, and P. D. Ye, Chloride molecular doping technique on 2D materials: WS_2 and MoS_2, *Nano Lett.* 14(11), 6275 (2014)
47. Y. Yoon, K. Ganapathi, and S. Salahuddin, How good can monolayer MoS_2 transistors Be? *Nano Lett.* 11(9), 3768 (2011)
48. Y. J. Zhang, J. T. Ye, Y. Matsuhashi, and Y. Iwasa, Ambipolar MoS_2 thin flake transistors, *Nano Lett.* 12(3), 1136 (2012)
49. K. Kaasbjerg, K. S. Thygesen, and K. W. Jacobsen, Phonon-limited mobility in n-type single-layer MoS_2 from first principles, *Phys. Rev. B* 85(11), 115317 (2012)
50. B. Radisavljevic, M. B. Whitwick, and A. Kis, Correction to integrated circuits and logic operations based on single-layer MoS_2, *ACS Nano* 7(4), 3729 (2013)
51. H. Wang, L. L. Yu, Y. H. Lee, Y. M. Shi, A. Hsu, M. L. Chin, L. J. Li, M. Dubey, J. Kong, and T. Palacios, Integrated circuits based on bilayer MoS_2 transistors, *Nano Lett.* 12(9), 4674 (2012)
52. H. S. Lee, S. W. Min, Y. G. Chang, M. K. Park, T. Nam, H. Kim, J. H. Kim, S. Ryu, and S. Im, MoS_2 nanosheet phototransistors with thickness-modulated optical energy gap, *Nano Lett.* 12(7), 3695 (2012)
53. F. K. Perkins, A. L. Friedman, E. Cobas, P. M. Campbell, G. G. Jernigan, and B. T. Jonker, Chemical vapor sensing with monolayer MoS_2, *Nano Lett.* 13(2), 668 (2013)
54. R. S. Sundaram, M. Engel, A. Lombardo, R. Krupke, A. C. Ferrari, P. Avouris, and M. Steiner, Electroluminescence in single layer MoS_2, *Nano Lett.* 13(4), 1416 (2013)
55. H. Zhang, S. B. Lu, J. Zheng, J. Du, S. C. Wen, D. Y. Tang, and K. P. Loh, Molybdenum disulfide (MoS_2) as a broadband saturable absorber for ultra-fast photonics, *Opt. Express* 22(6), 7249 (2014)
56. R. Hao, J. M. Jin, X. L. Peng, and E. Li, Dynamic control of wideband slow wave in graphene based waveguides, *Opt. Lett.* 39(11), 3094 (2014)
57. H. Xia, H. Li, C. Lan, C. Li, X. Zhang, S. Zhang, and Y. Liu, Ultrafast erbium-doped fiber laser mode-locked by a CVD-grown molybdenum disulfide (MoS_2) saturable absorber, *Opt. Express* 22(14), 17341 (2014)
58. K. Wu, X. Y. Zhang, J. Wang, X. Li, and J. P. Chen, WS_2 as a saturable absorber for ultrafast photonic applications of mode-locked and Q-switched lasers, *Opt. Express* 23(9), 11453 (2015)
59. P. G. Yan, A. J. Liu, Y. S. Chen, H. Chen, S. C. Ruan, C. Y. Guo, S. F. Chen, I. L. Li, H. P. Yang, J. G. Hu, and G. Z. Cao, Microfiber-based WS_2-film saturable absorber for ultra-fast photonics, *Opt. Mater. Express* 5(3), 479 (2015)
60. M. Liu, X. W. Zheng, Y. L. Qi, H. Liu, A. P. Luo, Z. C. Luo, W. C. Xu, C. J. Zhao, and H. Zhang, Microfiber-based few-layer MoS_2 saturable absorber for 25 GHz passively harmonic mode-locked fiber laser, *Opt. Express* 22(19), 22841 (2014)
61. Z. Luo, Y. Huang, M. Zhong, Y. Li, J. Wu, B. Xu, H. Xu, Z. Cai, J. Peng, and J. Weng, 1-, 1.5-, and 2-μm fiber lasers Q-switched by a broadband few-layer MoS_2 Saturable Absorber, *J. Lightwave Technol.* 32(24), 4679 (2014)

62. L. K. Li, Y. J. Yu, G. J. Ye, Q. Q. Ge, X. D. Ou, H. Wu, D. L. Feng, X. H. Chen, and Y. B. Zhang, Black phosphorus field-effect transistors, *Nat. Nanotechnol.* 9(5), 372 (2014)
63. H. H. Churchill and P. Jarillo-Herrero, Phosphorus joins the family, *Nat. Nanotechnol.* 9(5), 330 (2014)
64. H. Liu, A. T. Neal, Z. Zhu, Z. Luo, X. Xu, D. Tomanek, and P. D. Ye, Phosphorene: An Unexplored 2D semiconductor with a high hole mobility, *ACS Nano* 8(4), 4033 (2014)
65. M. Buscema, D. J. Groenendijk, S. I. Blanter, G. A. Steele, H. S. J. van der Zant, and A. Castellanos-Gomez, Fast and broadband photoresponse of few-layer black phosphorus field-effect transistors, *Nano Lett.* 14(6), 3347 (2014)
66. N. Junhong, L. Young Tack, L. Jung Ah, H. Do Kyung, K. Gyu-Tae, C. Won Kook, and S. Yong-Won, Few-layer black phosphorus field-effect transistors with reduced current fluctuation, *ACS Nano,* 8(11), 11753 (2014)
67. Z. B. Yang, J. H. Hao, S. G. Yuan, S. H. Lin, H. M. Yau, J. Y. Dai, and S. P. Lau, Field-effect transistors based on amorphous black phosphorus ultrathin films by pulsed laser deposition, *Adv. Mater.* 27(25), 3748 (2015)
68. T. Hong, B. Chamlagain, W. Z. Lin, H. J. Chuang, M. H. Pan, Z. X. Zhou, and Y. Q. Xu, Polarized photocurrent response in black phosphorus field-effect transistors, *Nanoscale* 6(15), 8978 (2014)
69. Z. Guo, S. Chen, Z. Wang, Z. Yang, F. Liu, Y. Xu, J. Wang, Y. Yi, H. Zhang, L. Liao, P. K. Chu, and X. F. Yu, Metal-ion-modified black phosphorus with enhanced stability and transistor performance, *Adv. Mater.* 29, (2017)
70. Y. Zhou, M. Zhang, Z. Guo, L. Miao, S. T. Han, Z. Wang, X. Zhang, H. Zhang, and Z. Peng, Recent advances in black phosphorus-based photonics, electronics, sensors and energy devices, *Mater. Horiz.* 4(6), 997 (2017)
71. M. Qiu, Z. T. Sun, D. K. Sang, X. G. Han, H. Zhang, and C. M. Niu, Current progress in black phosphorus materials and their applications in electrochemical energy storage, *Nanoscale* 9(36), 13384 (2017)
72. Y. Xu, J. Yuan, K. Zhang, Y. Hou, Q. Sun, Y. Yao, S. Li, Q. Bao, H. Zhang, and Y. Zhang, Field-induced n-doping of black phosphorus for CMOS compatible 2D logic electronics with high electron mobility, *Adv. Funct. Mater.* 27(38), 1702211 (2017)
73. M. Buscema, D. J. Groenendijk, S. I. Blanter, G. A. Steele, H. S. J. van der Zant, and A. Castellanos-Gomez, Fast and broadband photoresponse of few-layer black phosphorus field-effect transistors, *Nano Lett.* 14(6), 3347 (2014)
74. N. Youngblood, C. Chen, S. J. Koester, and M. Li, Waveguide-integrated black phosphorus photodetector with high responsivity and low dark current, *Nat. Photonics* 9(4), 247 (2015)
75. H. T. Yuan, X. G. Liu, F. Afshinmanesh, W. Li, G. Xu, J. Sun, B. Lian, A. G. Curto, G. J. Ye, Y. Hikita, Z. X. Shen, S. C. Zhang, X. H. Chen, M. Brongersma, H. Y. Hwang, and Y. Cui, Polarization-sensitive broadband photodetector using a black phosphorus vertical p–n junction, *Nat. Nanotechnol.* 10(8), 707 (2015)
76. J. S. Qiao, X. H. Kong, Z. X. Hu, F. Yang, and W. Ji, High-mobility transport anisotropy and linear dichroism in few-layer black phosphorus, *Nat. Commun.* 5, 4475 (2014)
77. Y. Li, S. Yang, and J. Li, Modulation of the electronic properties of ultrathin black phosphorus by strain and electrical field, *J. Phys. Chem. C* 118(41), 23970 (2014)
78. J. Dai and X. C. Zeng, Bilayer phosphorene, *J. Phys. Chem. Lett.* 5(7), 1289 (2014)
79. A. Zhuang, J. J. Li, Y. C. Wang, X. Wen, Y. Lin, B. Xiang, X. Wang, and J. Zeng, Screw-dislocation-driven bidirectional spiral growth of Bi_2Se_3 nanoplates, *Angew. Chem. Int. Ed. Engl.* 53(25), 6425 (2014)
80. M. Z. Hasan and C. L. Kane, Topological insulators, *Rev. Mod. Phys.* 82(4), 3045 (2010)
81. C. Y. Chen, Z. J. Xie, Y. Feng, H. M. Yi, A. J. Liang, S. L. He, D. X. Mou, J. F. He, Y. Y. Peng, X. Liu, Y. Liu, L. Zhao, G. D. Liu, X. L. Dong, J. Zhang, L. Yu, X. Y. Wang, Q. J. Peng, Z. M. Wang, S. J. Zhang, F. Yang, C. T. Chen, Z. Y. Xu, and X. J. Zhou, Tunable Dirac fermion dynamics in topological insulators, *Sci. Rep.* 3(10), 2411 (2013)
82. C. J. Zhao, Y. H. Zou, Y. Chen, Z. T. Wang, S. B. Lu, H. Zhang, S. C. Wen, and D. Y. Tang, Wavelength-tunable picosecond soliton fiber laser with topological insulator: Bi_2Se_3 as a mode locker: Erratum, *Opt. Express* 21(1), 444 (2013)
83. H. Zhang, X. He, W. Lin, R. Wei, F. Zhang, X. Du, G. Dong, and J. Qiu, Ultrafast saturable absorption in topological insulator Bi_2SeTe_2 nanosheets, *Opt. Express* 23(10), 13376 (2015)
84. X. He, H. Zhang, W. Lin, R. Wei, J. Qiu, M. Zhang, and B. Hu, PVP-assisted solvothermal synthesis of high-yielded Bi_2Te_3 hexagonal nanoplates: Application in passively Q-switched fiber laser, *Sci. Rep.* 5(1), 15868 (2015)
85. H. H. Yu, H. Zhang, Y. C. Wang, C. J. Zhao, B. L. Wang, S. C. Wen, H. J. Zhang, and J. Y. Wang, Topological insulator as an optical modulator for pulsed solid-state lasers, *Laser Photon. Rev.* 7(6), L77 (2013)
86. H. Huang, Y. Li, Q. Li, B. Li, Z. Song, W. Huang, C. Zhao, H. Zhang, S. Wen, D. Carroll, and G. Fang, Field electron emission of layered Bi_2Se_3 nanosheets with atom-thick sharp edges, *Nanoscale* 6(14), 8306 (2014)
87. Y. Tan, H. Zhang, C. Zhao, S. Akhmadaliev, S. Zhou, and F. Chen, Bi_2Se_3 Q-switched Nd:YAG ceramic waveguide laser, *Opt. Lett.* 40(4), 637 (2015)
88. X. Jiang, S. Gross, H. Zhang, Z. Guo, M. J. Withford, and A. Fuerbach, Bismuth telluride topological insulator nanosheet saturable absorbers for Q-switched mode-locked Tm:ZBLAN waveguide lasers, *Ann. Phys.* 528(7–8), 543 (2016)
89. M. Liu, Z. R. Cai, S. Hu, A. P. Luo, C. J. Zhao, H. Zhang, W. C. Xu, and Z. C. Luo, Dissipative rogue waves induced by long-range chaotic multi-pulse interactions in a fiber laser with a topological insulator-deposited microfiber photonic device, *Opt. Lett.* 40(20), 4767 (2015)
90. C. R. Ast and H. Hochst, Electronic structure of a bismuth bilayer, *Phys. Rev. B* 67(11), 181 (2003)

91. Y. M. Koroteev, G. Bihlmayer, J. E. Gayone, E. V. Chulkov, S. Blugel, P. M. Echenique, and P. Hofmann, Strong spin–orbit splitting on Bi surfaces, *Phys. Rev. Lett.* 93(4), 046403 (2004)
92. E. J. Tichovolsky and J. G. Mavroides, Magnetoreflection studies on the band structure of bismuth-antimony alloys, *Solid State Commun.* 7(13), 927 (1969)
93. Y. Ohtsubo, L. Perfetti, M. O. Goerbig, P. Le Fevre, F. Bertran, and A. Taleb-Ibrahimi, Non-trivial surface-band dispersion on bi(111), *New J. Phys.* 15, 033041 (2013)
94. L. Li, J. G. Checkelsky, Y. S. Hor, C. Uher, A. F. Hebard, R. J. Cava, and N. P. Ong, Phase transitions of Dirac electrons in bismuth, *Science* 321(5888), 547 (2008)
95. S. Murakami, Quantum spin Hall effect and enhanced magnetic response by spin–orbit coupling, *Phys. Rev. Lett.* 97(23), 236805 (2006)
96. J. P. Issi, Low temperature transport properties of the group V semimetals, *Aust. J. Phys.* 32(6), 585 (1979)
97. P. Hofmann, The surfaces of bismuth: Structural and electronic properties, *Prog. Surf. Sci.* 81(5), 191 (2006)
98. Y. Guo, Y. F. Zhang, X. Y. Bao, T. Z. Han, Z. Tang, L. X. Zhang, W. G. Zhu, E. G. Wang, Q. Niu, Z. Q. Qiu, J. F. Jia, Z. X. Zhao, and Q. K. Xue, Superconductivity modulated by quantum size effects, *Science* 306(5703), 1915 (2004)
99. L. Lu, Z. M. Liang, L. M. Wu, Y. X. Chen, Y. F. Song, S. C. Dhanabalan, J. S. Ponraj, B. Q. Dong, Y. J. Xiang, F. Xing, D. Y. Fan, and H. Zhang, Few-layer bismuthene: Sonochemical exfoliation, nonlinear optics and applications for ultrafast photonics with enhanced stability, *Laser Photon. Rev.* 12(1), 1870012 (2018)
100. J. Wang, Y. Hernandez, M. Lotya, J. N. Coleman, and W. J. Blau, Broadband nonlinear optical response of graphene dispersions, *Adv. Mater.* 21(23), 2430 (2009)
101. H. H. Yu, X. F. Chen, H. J. Zhang, X. G. Xu, X. B. Hu, Z. P. Wang, J. Y. Wang, S. D. Zhuang, and M. H. Jiang, Large energy pulse generation modulated by graphene epitaxially grown on silicon carbide, *ACS Nano* 4(12), 7582 (2010)
102. H. Zhang, D. Tang, R. J. Knize, L. Zhao, Q. Bao, and K. P. Loh, Graphene mode locked, wavelength-tunable, dissipative soliton fiber laser, *Appl. Phys. Lett.* 96(11), 111112 (2010)
103. J. Tang, Y. Chen, Y. Lin, X. Gong, J. Huang, Z. Luo, and Y. Huang, Tm^3/Ho^{3+} co-doped $LiGd(MoO_4)_2$ crystal as laser gain medium around 20 μm, *Opt. Mater. Express* 2(8), 878 (2012)
104. Z. W. Zheng, C. J. Zhao, S. B. Lu, Y. Chen, Y. Li, H. Zhang, and S. C. Wen, Microwave and optical saturable absorption in graphene, *Opt. Express* 20(21), 23201 (2012)
105. E. Hendry, P. J. Hale, J. Moger, A. K. Savchenko, and S. A. Mikhailov, Coherent nonlinear optical response of graphene, *Phys. Rev. Lett.* 105(9), 097401 (2010)
106. M. B. M. Krishna, V. P. Kumar, N. Venkatramaiah, R. Venkatesan, and D. N. Rao, Nonlinear optical properties of covalently linked graphene-metal porphyrin composite materials, *Appl. Phys. Lett.* 98(8), 081106 (2011)
107. W. Chen, G. Wang, S. Qin, C. Wang, J. Fang, J. Qi, X. Zhang, L. Wang, H. Jia, and S. Chang, The nonlinear optical properties of coupling and decoupling graphene layers, *AIP Adv.* 3(4), 042123 (2013)
108. K. Wang, J. Wang, J. Fan, M. Lotya, A. O' Neill, D. Fox, Y. Feng, X. Zhang, B. Jiang, Q. Zhao, H. Zhang, J. N. Coleman, L. Zhang, and W. J. Blau, Ultrafast saturable absorption of two-dimensional MoS_2 nanosheets, *ACS Nano* 7(10), 9260 (2013)
109. X. Zhang, S. Zhang, C. Chang, Y. Feng, Y. Li, N. Dong, K. Wang, L. Zhang, W. J. Blau, and J. Wang, Facile fabrication of wafer-scale MoS_2 neat films with enhanced third-order nonlinear optical performance, *Nanoscale* 7(7), 2978 (2015)
110. A. Splendiani, L. Sun, Y. Zhang, T. Li, J. Kim, C. Y. Chim, G. Galli, and F. Wang, Emerging photoluminescence in monolayer MoS_2, *Nano Lett.* 10(4), 1271 (2010)
111. A. Pulkin and O. V. Yazyev, Spin- and valley-polarized transport across line defects in monolayer MoS_2, *Phys. Rev. B* 93(4), 041419 (2016)
112. Q. Ouyang, H. Yu, K. Zhang, and Y. Chen, Saturable absorption and the changeover from saturable absorption to reverse saturable absorption of MoS_2 nanoflake array films, *J. Mater. Chem. C* 2(31), 6319 (2014)
113. K. G. Zhou, M. Zhao, M. J. Chang, Q. Wang, X. Z. Wu, Y. Song, and H. L. Zhang, Size-dependent nonlinear optical properties of atomically thin transition metal dichalcogenide nanosheets, *Small* 11(6), 694 (2015)
114. D. Mao, Y. Wang, C. Ma, L. Han, B. Jiang, X. Gan, S. Hua, W. Zhang, T. Mei, and J. Zhao, WS_2 mode-locked ultrafast fiber laser, *Sci. Rep.* 5(1), 7965 (2015)
115. R. F. Wei, H. Zhang, Z. L. Hu, T. Qiao, X. He, Ultrabroadband nonlinear saturable absorption of high-yield MoS_2 nanosheets, *Nanotechnology* 27(30), 305203 (2016)
116. F. Bernard, Z. Han, S. P. Gorza, and P. Emplit, Towards mode-locked fiber laser using topological insulators, *Nonlin. Photon.* 5, 2012
117. C. J. Zhao, Y. H. Zou, Y. Chen, Z. T. Wang, S. B. Lu, H. Zhang, S. C. Wen, and D. Y. Tang, Wavelength-tunable picosecond soliton fiber laser with topological insulator: Bi_2Se_3 as a mode locker, *Opt. Express* 20(25), 27888 (2012)
118. C. J. Zhao, H. Zhang, X. Qi, Y. Chen, Z. T. Wang, S. C. Wen, and D. Y. Tang, Ultra-short pulse generation by a topological insulator based saturable absorber, *Appl. Phys. Lett.* 101(21), 118(2012)
119. S. B. Lu, C. J. Zhao, Y. H. Zou, S. Q. Chen, Y. Chen, Y. Li, H. Zhang, S. C. Wen, and D. Y. Tang, Third order nonlinear optical property of Bi_2Se_3, *Opt. Express* 21(2), 2072 (2013)
120. Z. Q. Luo, C. Liu, Y. Z. Huang, D. D. Wu, J. Y. Wu, H. Y. Xu, Z. P. Cai, Z. Q. Lin, L. P. Sun, and J. Weng, Topological-insulator passively Q-switched double-clad fiber laser at 2 μm wavelength, *IEEE J. Sel. Top. Quant.* 902708 2014, 20(5)
121. M. Jung, J. Lee, J. Koo, J. Park, Y. W. Song, K. Lee, S. Lee, and J. H. Lee, A femtosecond pulse fiber laser at 1935 nm using a bulk-structured Bi_2Te_3 topological insulator, *Opt. Express* 22(7), 7865 (2014)

122. B. Weitzel and H. Micklitz, Superconductivity in granular systems built from well-defined rhombohedral Bi-clusters: Evidence for Bi-surface superconductivity, *Phys. Rev. Lett.* 66(3), 385 (1991)

123. L. Gui, X. Li, X. Xiao, H. Zhu, and C. Yang, Widely spaced bound states in a soliton fiber laser with graphene saturable absorber, *IEEE Photon. Technol. Lett.* 25(12), 1184 (2013)

124. L. Cheng, H. Liu, X. Tan, J. Zhang, J. Wei, and H. Lv, Thermoelectric properties of a monolayer bismuth, *J. Phys. Chem. C* 118(2), 904 (2014)

125. Y. M. Koroteev, G. Bihlmayer, E. V. Chulkov, and S. Blügel, First-principles investigation of structural and electronic properties of ultrathin Bi films, *Phys. Rev. B* 77(4), 045428 (2008)

126. B. Guo, S. H. Wang, Z. X. Wu, Z. X. Wang, D. H. Wang, H. Huang, F. Zhang, Y. Q. Ge, and H. Zhang, Sub-200 fs soliton mode-locked fiber laser based on bismuthene saturable absorber, *Opt. Express* 26(18), 22750 (2018)

127. Q. Q. Yang, R. T. Liu, C. Huang, Y. F. Huang, L. F. Gao, B. Sun, Z. P. Huang, L. Zhang, C. X. Hu, Z. Q. Zhang, C. L. Sun, Q. Wang, Y. L. Tang, and H. L. Zhang, 2D bismuthene fabricated via acid-intercalated exfoliation showing strong nonlinear near-infrared responses for mode-locking lasers, *Nanoscale* 10(45), 21106 (2018)

128. P. Zijlstra, J. W. Chon, and M. Gu, Five-dimensional optical recording mediated by surface plasmons in gold nanorods, *Nature* 459(7245), 410 (2009)

129. D. Tan, Y. Yamada, S. Zhou, Y. Shimotsuma, K. Miura, and J. Qiu, Carbon nanodots with strong nonlinear optical response, *Carbon* 69, 638 (2014)

130. R. L. Gieseking, S. Mukhopadhyay, C. Risko, and J. L. Brédas, Impact of the nature of the excited-state transition dipole moments on the third-order nonlinear optical response of polymethine dyes for all-optical switching applications, *ACS Photon.* 1(3), 261 (2014)

131. W. Man, C. Yu, Z. Han, and W. Shuangchun, Nanosecond Q-switched erbium-doped fiber laser with wide pulse-repetition-rate range based on topological insulator, *IEEE J. Quantum Electron.* 50, 393 (2014)

132. Y. Chen, C. Zhao, S. Chen, J. Du, P. Tang, G. Jiang, H. Zhang, S. Wen, and D. Tang, Large energy, wavelength widely tunable, topological insulator Q-switched erbium-doped fiber laser, *IEEE J. Sel. Top. Quantum Electron.* 20(5), 315 (2014)

133. F. Yan, W. Peng, S. Liu, T. Feng, Z. Dong, and G. K. Chang, Dual-wavelength single-longitudinal-mode tm-doped fiber laser using PM-CMFBG, *IEEE Photonics Technol. Lett.* 27(9), 264 (2015)

134. C. Li, J. Liu, Z. Guo, H. Zhang, W. Ma, J. Wang, X. Xu, and L. Su, Black phosphorus saturable absorber for a diode-pumped passively Q-switched Er:CaF_2 mid-infrared laser, *Opt. Commun.* 406, 158 (2018)

135. P. Ge, J. Liu S. Jiang, Y. Xu, and B. Man, Compact Q-switched 2 m Tm:$GdVO_4$ laser with MoS_2 absorber, *Photon. Res.* 3(5), 256 (2015)

136. J. Liu, J. Liu, Z. Guo, H. Zhang, W. Ma, J. Wang, and L. Su, Dual-wavelength Q-switched Er:SrF_2 laser with a black phosphorus absorber in the mid-infrared region, *Opt. Express* 24(26), 30289 (2016)

137. Y. Zhao, P. L. Guo, X. H. Li, and Z. W. Jin, Ultrafast photonics application of graphdiyne in the optical communication region, *Carbon* 149, 336 (2019)

138. T. C. Feng, X. H. Li, T. Chai, P. L. Guo, Y. Zhang, R. S. Liu, J. S. Liu, J. B. Lu, and Y. Q. Ge, Bismuthene nanosheets for 1-μm multipulse generation, *Langmuir* 36(1), 3 (2020)

139. Z. J. Shi, W. X. Xu, X. H. Li, and Z. Hui, Cuprous sulfide for different laser pulse generation: Q-switching and mode-locking, *J. Phys. Chem. C* 123(46), 28370 (2019)

140. J. Feng, X. Li, Z. Shi, C. Zheng, X. Li, D. Leng, Y. Wang, J. Liu, and L. Zhu, 2D ductile transition metal chalcogenides (TMCs): A novel hiah-performance Ag_2S nanosheets for ultrafast photonics, *Adv. Opt. Mater.* 8(6), 1901762 (2020)

141. J. S. Liu, X. H. Li, Y. X. Guo, A. Qyyum, Z. J. Shi, T. C. Feng, Y. Zhang, C. X. Jiang, and X. F. Liu, $SnSe_2$ nanosheets for subpicosecond harmonic mode-locked pulse generation, *Small* 15(38), 1902811 (2019)

142. T. C. Feng, D. Zhang, X. H. Li, Q. Abdul, Z. J. Shi, J. B. Lu, P. L. Guo, Y. Zhang, J. S. Liu, and Q. J. Wang, SnS_2 nanosheets for Er-doped fiber lasers, *ACS Appl. Nanomater. (Basel)* 3(1), 674 (2020)

143. X. H. Li, X. C. Yu, Z. P. Sun, Z. Y. Yan, B. Sun, Y. B. Cheng, X. Yu, Y. Zhang, and Q. J. Wang, High-power graphene mode-locked Tm/Ho co-doped fiber laser with evanescent field interaction, *Sci. Rep.* 5(1), 16624 (2015)

144. X. H. Li, K. Wu, Z. P. Sun, B. Meng, Y. G. Wang, Y. S. Wang, X. C. Yu, X. Yu, Y. Zhang, P. P. Shum, and Q. J. Wang, Single-wall carbon nanotubes and graphene oxide-based saturable absorbers for low phase noise mode-locked fiber lasers, *Sci. Rep.* 6(1), 25266 (2016)

145. L. M. Zhao, D. Y. Tang, X. Wu, H. Zhang, and H. Y. Tam, Coexistence of polarization-locked and polarization-rotating vector solitons in a fiber laser with SESAM, *Opt. Lett.* 34(20), 3059 (2009)

146. L. M. Zhao, D. Y. Tang, H. Zhang, and X. Wu, Polarization rotation locking of vector solitons in a fiber ring laser, *Opt. Express* 16(14), 10053 (2008)

147. L. M. Zhao, D. Y. Tang, H. Zhang, X. Wu, and N. Xiang, Soliton trapping in fiber lasers, *Opt. Express* 16(13), 9528 (2008)

148. H. Zhang, D. Y. Tang, L. M. Zhao, and H. Y. Tam, Induced solitons formed by cross-polarization coupling in a birefringent cavity fiber laser, *Opt. Lett.* 33(20), 2317 (2008)

149. L. M. Zhao, D. Y. Tang, X. Wu, and H. Zhang, Dissipative soliton trapping in normal dispersion-fiber lasers, *Opt. Lett.* 35(11), 1902 (2010)

150. L. M. Zhao, D. Y. Tang, H. Zhang, and X. Wu, Bunch of restless vector solitons in a fiber laser with SESAM, *Opt. Express* 17(10), 8103 (2009)

151. J. Ma, Z. Qin, G. Xie, L. Qian, and D. Tang, Review of mid-infrared mode-locked laser sources in the 2.0–3.5 μm spectral region, *Appl. Phys. Rev.* 6(2), 021317 (2019)

152. G. Chang and Z. Wei, Ultrafast fiber lasers: An expanding versatile toolbox, *iScience* 23(5) 101101 (2020)
153. C. Shang, Y. Zhang, H. Qin, B. He, C. Zhang, J. Sun, J. Li, J. Ma, X. Ji, L. Xu, and B. Fu., Review on wavelength-tunable pulsed fiber lasers based on 2D materials, *Opt. Laser Technol.* 131, 106375 (2020)
154. Y. Han, Y. Guo, B. Gao, C. Ma, H. Zhang, and H. Zhang, Generation, optimization, and application of ultrashort femtosecond pulse in mode-locked fiber lasers, *Prog. Quantum Electron.* 71, 100264 (2020)
155. T. Jiang, K. Yin, C. Wang, J. You, H. Ouyang, R. Miao, C. Zhang, K. Wei, H. Li, H. Chen, R. Zhang, X. Zheng, Z. Xu, X. Cheng, and H. Zhang, Ultrafast fiber lasers mode-locked by two-dimensional materials: Review and prospect, *Photon. Res.* 8(1), 78 (2020)
156. P. L. Huang, S. Lin, C. Yeh, H. Kuo, S. Huang, G. Lin, L. Li, C. Su, and W. Cheng, Stable mode-locked fiber laser based on CVD fabricated graphene saturable absorber, *Opt. Express* 20(3), 2460 (2012)
157. Z. Zheng, C. Zhao, S. Lu, Y. Chen, H. Li, Y. Zhang, and S. Wen, Microwave and optical saturable absorption in graphene, *Opt. Express* 20(21), 23201 (2012)
158. B. Fu, Y. Hua, X. Xiao, H. Zhu, Z. Sun, and C. Yang, Broadband graphene saturable absorber for pulsed fiber lasers at 1, 1.5, and 2 mm, *IEEE J. Sel. Top. Quantum Electron.* 20(5), 1100705 (2014)
159. L. Liu, H. T. Hattori, E. G. Mironov, and A. Khaleque, Composite chromium and graphene oxide as saturable absorber in ytterbium-doped Q-switched fiber lasers, *Appl. Opt.* 53(6), 1173 (2014)
160. L. Li, X. Zheng, X. Chen, M. Qi, Z. Ren, J. Bai, and Z. Sun, High-power diode-side-pumped Nd:YAG solid laser mode-locked by CVD graphene, *Opt. Comm.* 315, 204 (2014)
161. X. Li, W. Zou, and J. Chen, 419 fs hybridly mode-locked Er-doped fiber laser at 212 MHz repetition rate, *Opt. Lett.* 39(6), 1553 (2014)
162. Q. Wen, X. Zhang, Y. Wang, Y. Wang, and H. Niu, Passively Q-switched Nd:YAG laser with graphene oxide in heavy water, *IEEE Photon. J.* 6(2), 1 (2014)
163. J. Xu, S. Wu, J. Liu, Y. Li, J. Ren, Q. H. Yang, and P. Wang, All-polarization-maintaining femtosecond fiber lasers using graphene oxide saturable absorber, *IEEE Photon. Technol. Lett.* 26(4), 346 (2014)
164. X. He, D. N. Wang, and Z. B. Liu, Pulse-width tuning in a passively mode-locked fiber laser with graphene saturable absorber, *IEEE Photon. Technol. Lett.* 26(4), 360 (2014)
165. Y. Chen, G. Jiang, S. Chen, Z. Guo, X. Yu, C. Zhao, H. Zhang, Q. Bao, S. Wen, D. Tang, and D. Fan, Mechanically exfoliated black phosphorus as a new saturable absorber for both Q-switching and mode-locking laser operation, *Opt. Express* 23(10), 12823 (2015)
166. F. Zhang, Z. Wu, Z. Wang, D. Wang, S. Wang, and X. Xu, Strong optical limiting behavior discovered in black phosphorus, *RSC Adv.* 6(24), 20027 (2016)
167. F. Zhang, Z. Wang, D. Wang, Z. Wu, S. Wang, and X. Xu, Nonlinear optical effects in nitrogen-doped graphene, *RSC Adv.* 6(5), 3526 (2016)
168. J. L. Wu, B. Gu, N. Sheng, D. Liu, and Y. Cui, Enhanced optical limiting effects in a double-decker bis(phthalocyaninato) rare earth complex using radially polarized beams, *Appl. Phys. Lett.* 105(17), 171113 (2014)
169. C. Zheng, W. Chen, S. Cai, X. Xiao, and X. Ye, Enhanced optical limiting properties of graphene oxide/triangular Pd nanocrystal composites, *Mater. Lett.* 131, 284 (2014)
170. A. A. Ryzhov, I. M. Belousova, Y. Wang, H. Qi, and J. Wang, Optical limiting properties of a nonlinear multilayer Fabry–Perot resonator containing niobium pentoxide as nonlinear medium, *Opt. Lett.* 39(16), 4847 (2014)
171. A. Diallo, S. Zongo, P. Mthunzi, S. Rehman, S. Y. Alqaradawi, W. Soboyejo, and M. Maaza, Z-scan and optical limiting properties of Hibiscus Sabdariffa dye, *Appl. Phys. B* 117(3), 861 (2014)
172. I. Papagiannouli, A. B. Bourlinos, A. Bakandritsos, and S. Couris, Nonlinear optical properties of colloidal carbon nanoparticles: Nanodiamonds and carbon dots, *RSC Advances* 4(76), 40152 (2014)
173. P. Aloukos, I. Papagiannouli, A. B. Bourlinos, R. Zboril, and S. Couris, Third-order nonlinear optical response and optical limiting of colloidal carbon dots, *Opt. Express* 22(10), 12013 (2014)
174. M. J. Weber, D. Milam, and W. L. Smith, Nonlinear refractive index of glasses and crystals, *Opt. Eng.* 17(5), 463 (1978)
175. R. Adair, L. L. Chase, and S. A. Payne, Nonlinear refractive-index measurements of glasses using three-wave frequency mixing, *J. Opt. Soc. Anier. B* 4(6), 875 (1987)
176. C. Cheng, Z. Li, N. Dong, J. Wang, and F. Chen, Tin diselenide as a new saturable absorber for generation of laser pulses at 1 m, *Opt. Express* 25(6), 6132 (2017)
177. S. L. Wong, H. Liu, and D. Chi, Recent progress in chemical vapor deposition growth of two-dimensional transition metal dichalcogenides, *Prog. Cryst. Growth Charact. Mater.* 62(3), 9 (2016)
178. K. Yan, L. Fu, H. L. Peng, and Z. F. Liu, Designed CVD growth of graphene via process engineering, *Acc. Chem. Res.* 46(10), 2263 (2013)
179. D. Hanlon, C. Backes, E. Doherty, C. S. Cucinotta, N. C. Berner, C. Boland, K. Lee, A. Harvey, P. Lynch, Z. Gholamvand, S. Zhang, K. Wang, G. Moynihan, A. Pokle, Q. M. Ramasse, N. McEvoy, W. J. Blau, J. Wang, G. Abellan, F. Hauke, A. Hirsch, S. Sanvito, D. D. O′ Regan, G. S. Duesberg, V. Nicolosi, and J. N. Coleman, Liquid exfoliation of solvent-stabilized few-layer black phosphorus for applications beyond electronics, *Nat. Commun.* 6(1), 8563 (2015)
180. H. Li, G. Lu, Y. Wang, Z. Yin, C. Cong, Q. He, L. Wang, F. Ding, T. Yu, and H. Zhang, Mechanical exfoliation and characterization of single- and few-layer nanosheets of WSe_2, TaS_2, and $TaSe_2$, *Small* 9(11), 1974 (2013)
181. A. Castellanos-Gomez, L. Vicarelli, E. Prada, J. O. Island, K. L. Narasimha-Acharya, S. I. Blanter, D. J. Groenendijk, M. Buscema, G. A. Steele, J. V. Alvarez, H. W. Zandbergen, J. J. Palacios, and H. S. J. van der Zant, Isolation and characterization of few-layer black phosphorus, *2D Mater.* 1, 025001 (2014)

182. S. S. Hong, W. Kundhikanjana, J. J. Cha, K. Lai, D. Kong, S. Meister, M. A. Kelly, Z. X. Shen, and Y. Cui, Ultrathin topological insulator Bi_2Se_3 nanoribbons exfoliated by atomic force microscopy, *Nano Lett.* 10(8), 3118 (2010)

183. L. H. Li, Y. Chen, G. Behan, H. Zhang, M. Petravic, and A. M. Glushenkov, Large-scale mechanical peeling of boron nitride nanosheets by low-energy ball milling, *J. Mater. Chem.* 21(32), 11862 (2011)

184. D. R. Dreyer, S. Park, C. W. Bielawski, and R. S. Ruoff, The chemistry of graphene oxide, *Chem. Soc. Rev.* 39(1), 228 (2010)

185. J. M. Hughes, D. Aherne, and J. N. Coleman, Generalizing solubility parameter theory to apply to one- and two-dimensional solutes and to incorporate dipolar interactions, *J. Appl. Polym. Sci.* 127(6), 4483 (2013)

186. Y. Hernandez, M. Lotya, D. Rickard, S. D. Bergin, and J. N. Coleman, Measurement of multicomponent solubility parameters for graphene facilitates solvent discovery, *Langmuir* 26(5), 3208 (2010)

187. A. O' Neill, U. Khan, P. N. Nirmalraj, J. Boland, and J. N. Coleman, Graphene dispersion and exfoliation in low boiling point solvents, *J. Phys. Chem. C* 115(13), 5422 (2011)

188. A. B. Bourlinos, V. Georgakilas, R. Zboril, T. A. Steriotis, and A. K. Stubos, Liquid-phase exfoliation of graphite towards solubilized graphenes, *Small* 5(16), 1841 (2009)

189. G. Z. Magda, J. Peto, G. Dobrik, C. Hwang, L. P. Biro, and L. Tapaszto, Exfoliation of large-area transition metal chalcogenide single layers, *Sci. Rep.* 5(1), 14714 (2015)

190. J. Zheng, H. Zhang, S. Dong, Y. Liu, C. T. Nai, H. S. Shin, H. Y. Jeong, B. Liu, and K. P. Loh, High yield exfoliation of two-dimensional chalcogenides using sodium naphthalenide, *Nat. Commun.* 5(1), 2995 (2014)

191. G. Cunningham, M. Lotya, C. S. Cucinotta, S. Sanvito, S. D. Bergin, R. Menzel, M. S. P. Shaffer, and J. N. Coleman, Solvent exfoliation of transition metal dichalcogenides: Dispersibility of exfoliated nanosheets varies only weakly between compounds, *ACS Nano* 6(4), 3468 (2012)

192. J. R. Brent, N. Savjani, E. A. Lewis, S. J. Haigh, D. J. Lewis, and P. O′ Brien, Production of few-layer phosphorene by liquid exfoliation of black phosphorus, *Chem. Commun. (Camb.)* 50(87), 13338 (2014)

193. J. Kang, J. D. Wood, S. A. Wells, J. H. Lee, X. L. Liu, K. S. Chen, and M. C. Hersam, Solvent exfoliation of electronic-grade, two-dimensional black phosphorus, *ACS Nano* 9(4), 3596 (2015)

194. Y. Lin, T. V. Williams, and J. W. Connell, Soluble, exfoliated hexagonal boron nitride nanosheets, *J. Phys. Chem. Lett.* 1(1), 277 (2010)

195. D. Yoo, M. Kim, S. Jeong, J. Han, and J. Cheon, Chemical synthetic strategy for single-layer transition-metal chalcogenides, *J. Am. Chem. Soc.* 136(42), 14670 (2014)

196. A. N. Obraztsov, Making graphene on a large scale, *Nat. Nanotechnol.* 4(4), 212 (2009)

197. T. Niu, M. Zhou, J. Zhang, Y. Feng, and W. Chen, Growth intermediates for CVD graphene on Cu(111): Carbon clusters and defective graphene, *J. Am. Chem. Soc.* 135(22), 8409 (2013)

198. S. Tang, H. Wang, H. S. Wang, Q. Sun, X. Zhang, C. Cong, H. Xie, X. Liu, X. Zhou, F. Huang, X. Chen, T. Yu, F. Ding, X. Xie, and M. Jiang, Silane-catalysed fast growth of large single-crystalline graphene on hexagonal boron nitride, *Nat. Commun.* 6(1), 6499 (2015)

199. Y. Shi, C. Hamsen, X. Jia, K. K. Kim, A. Reina, M. Hofmann, A. L. Hsu, K. Zhang, H. Li, Z. Y. Juang, M. S. Dresselhaus, L. J. Li, and J. Kong, Synthesis of few-layer hexagonal boron nitride thin film by chemical vapor deposition, *Nano Lett.* 10(10), 4134 (2010)

200. S. Bae, H. Kim, Y. Lee, X. Xu, J.S. Park, Y. Zheng, J. Balakrishnan, T. Lei, H. Ri Kim, Y. I. Song, Y.J. Kim, K. S. Kim, B. Özyilmaz, J.H. Ahn, B. H. Hong, and S. Iijima., Roll-to-roll production of 30-inch graphene films for transparent electrodes, *Nat. Nanotechnol.* 5(8), 574 (2010)

201. Q. Yu, L. A. Jauregui, W. Wu, R. Colby, J. Tian, Z. Su, H. Cao, Z. Liu, D. Pandey, D. Wei, T. F. Chung, P. Peng, N. P. Guisinger, E. A. Stach, J. Bao, S. S. Pei, and Y. P. Chen, Control and characterization of individual grains and grain boundaries in graphene grown by chemical vapour deposition, *Nat. Mater.* 10(6), 443 (2011)

202. Y. Zhang, Y. F. Zhang, Q. Q. Ji, J. Ju, H. T. Yuan, J. P. Shi, T. Gao, D. L. Ma, M. X. Liu, Y. B. Chen, X. J. Song, H. Y. Hwang, Y. Cui, and Z. F. Liu, Controlled growth of high-quality monolayer WS_2 layers on sapphire and imaging its grain boundary, *ACS Nano* 7(10), 8963 (2013)

203. Y. Shi, W. Zhou, A. Y. Lu, W. Fang, Y. H. Lee, A. L. Hsu, S. M. Kim, K. K. Kim, H. Y. Yang, L. J. Li, J. C. Idrobo, and J. Kong, van der Waals epitaxy of MoS_2 layers using graphene as growth templates, *Nano Lett.* 12(6), 2784 (2012)

204. C. Cong, J. Shang, X. Wu, B. Cao, N. Peimyoo, C. Qiu, L. Sun, and T. Yu, Synthesis and optical properties of large-area single-crystalline 2D semiconductor WS_2 monolayer from chemical vapor deposition, *Adv. Opt. Mater.* 2(2), 131 (2014)

205. W. W. Piper and S. J. Polich, Vapor-phase growth of single crystals of II–VI compounds, *J. Appl. Phys.* 32(7), 1278 (1961)

206. H. Li, J. Cao, W. Zheng, Y. Chen, D. Wu, W. Dang, K. Wang, H. Peng, and Z. Liu, Controlled synthesis of topological insulator nanoplate arrays on mica, *J. Am. Chem. Soc.* 134(14), 6132 (2012)

207. Z. H. Sun and H. X. Chang, Graphene and graphene-like two-dimensional materials in photodetection: Mechanisms and methodology, *ACS Nano* 8(5), 4133 (2014)

208. D. Kong, W. Dang, J. J. Cha, H. Li, S. Meister, H. Peng, Z. Liu, and Y. Cui, Few-layer nanoplates of Bi_2Se_3 and Bi_2Te_3 with highly tunable chemical potential, *Nano Lett.* 10(6), 2245 (2010)

209. K. K. Kim, A. Hsu, X. Jia, S. M. Kim, Y. Shi, M. Hofmann, D. Nezich, J. F. Rodriguez-Nieva, M. Dresselhaus, T. Palacios, and J. Kong, Synthesis of monolayer hexagonal boron nitride on Cu foil using chemical vapor deposition, *Nano Lett.* 12(1), 161 (2012)

210. P. Sutter, J. Lahiri, P. Albrecht, and E. Sutter, Chemical vapor deposition and etching of high-quality monolayer hexagonal boron nitride films, *ACS Nano* 5(9), 7303 (2011)

211. K. H. Lee, H. J. Shin, J. Lee, I. Y. Lee, G. H. Kim, J. Y. Choi, and S. W. Kim, Large-scale synthesis of high-quality hexagonal boron nitride nanosheets for large-area graphene electronics, *Nano Lett.* 12(2), 714 (2012)

212. K. Ueno, K. Saiki, T. Shimada, and A. Koma, Epitaxial growth of transition metal dichalcogenides on cleaved faces of mica, *J. Vac. Sci. Technol. A* 8(1), 68 (1990)

213. Y. C. Lin, C. Y. Chang, R. K. Ghosh, J. Li, H. Zhu, R. Addou, B. Diaconescu, T. Ohta, X. Peng, N. Lu, M. J. Kim, J. T. Robinson, R. M. Wallace, T. S. Mayer, S. Datta, L. J. Li, and J. A. Robinson, Atomically thin heterostructures based on single-layer tungsten diselenide and graphene, *Nano Lett.* 14(12), 6936 (2014)

214. W. Yang, G. Chen, Z. Shi, C. C. Liu, L. Zhang, G. Xie, M. Cheng, D. Wang, R. Yang, D. Shi, K. Watanabe, T. Taniguchi, Y. Yao, Y. Zhang, and G. Zhang, Epitaxial growth of single-domain graphene on hexagonal boron nitride, *Nat. Mater.* 12(9), 792 (2013)

215. P. Yan, H. Chen, J. Yin, Z. Xu, J. Li, Z. Jiang, W. Zhang, J. Wang, I. L. Li, Z. Sun, and S. Ruan, Large-area tungsten disulfide for ultrafast photonics, *Nanoscale* 9(5), 1871 (2017)

216. A. Azizi, S. Eichfeld, G. Geschwind, K. H. Zhang, B. Jiang, D. Mukherjee, L. Hossain, A. F. Piasecki, B. Kabius, J. A. Robinson, and N. Alem, Freestanding van der Waals heterostructures of graphene and transition metal dichalcogenides, *ACS Nano* 9(5), 4882 (2015)

217. X. Liu, I. Balla, H. Bergeron, G. P. Campbell, M. J. Bedzyk, and M. C. Hersam, Rotationally commensurate growth of MoS_2 on epitaxial graphene, *ACS Nano* 10(1), 1067 (2016)

218. Y. F. Song, H. Zhang, D. Y. Tang, and D. Y. Shen, Polarization rotation vector solitons in a graphene mode-locked fiber laser, *Opt. Express* 20(24), 27283 (2012)

219. Y. Jiang, L. Miao, G. Jiang, Y. Chen, X. Qi, X. F. Jiang, H. Zhang, and S. Wen, Broadband and enhanced nonlinear optical response of MoS_2/graphene nanocomposites for ultrafast photonics applications, *Sci. Rep.* 5(1), 16372 (2015)

220. G. Zheng, Y. Chen, H. Huang, C. Zhao, S. Lu, S. Chen, H. Zhang, and S. Wen, Improved transfer quality of CVD-grown graphene by ultrasonic processing of target substrates: Applications for ultra-fast laser photonics, *ACS Appl. Mater. Interfaces* 5(20), 10288 (2013)

221. Z. T. Wang, Y. Chen, C. J. Zhao, H. Zhang, and S. C. Wen, Switchable dual-wavelength synchronously Q-switched erbium-doped fiber laser based on graphene saturable absorber, *IEEE Photon. J.* 4(3), 869 (2012)

222. Q. Bao, H. Zhang, Y. Wang, Z. Ni, Y. Yan, Z. X. Shen, K. P. Loh, and D. Y. Tang, Atomic-layer graphene as a saturable absorber for ultrafast pulsed lasers, *Adv. Funct. Mater.* 19(19), 3077 (2009)

223. M. Zhang, E. J. R. Kelleher, F. Torrisi, Z. Sun, T. Hasan, D. Popa, F. Wang, A. C. Ferrari, S. V. Popov, and J. R. Taylor, Tm-doped fiber laser mode-locked by graphene-polymer composite, *Opt. Express* 20(22), 25077 (2012).

224. D. Popa, Z. Sun, T. Hasan, F. Torrisi, F. Wang, and A. C. Ferrari, Graphene Q-switched, tunable fiber laser, *Appl. Phys. Lett.* 98(7), 073106 (2011)

225. X. Liu, Q. Guo, and J. Qiu, Emerging low-dimensional materials for nonlinear optics and ultrafast photonics, *Adv. Mater.* 29(14), 1605886 (2017)

226. S. Wang, H. Yu, H. Zhang, A. Wang, M. Zhao, Y. Chen, L. Mei, and J. Wang, Broadband few-layer MoS_2 saturable absorbers, *Adv. Mater.* 26(21), 3538 (2014)

227. H. Chen, X. Wen, J. Zhang, T. Wu, Y. Gong, X. Zhang, J. Yuan, C. Yi, J. Lou, P. M. Ajayan, W. Zhuang, G. Zhang, and J. Zheng, Ultrafast formation of interlayer hot excitons in atomically thin MoS_2/WS_2 heterostructures, *Nat. Commun.* 7(1), 12512 (2016)

228. P. Yan, H. Chen, J. Yin, Z. Xu, J. Li, Z. Jiang, W. Zhang, J. Wang, I. L. Li, Z. Sun, and S. Ruan, Large-area tungsten disulfide for ultrafast photonics, *Nanoscale* 9(5), 1871 (2017)

229. X. Li, S. Zhang, Y. Hao, and Z. Yang, Pulse bursts with a controllable number of pulses from a mode-locked Yb-doped all fiber laser system, *Opt. Express* 22(6), 6699 (2014)

230. Z. Wang, Y. Xu, S. C. Dhanabalan, J. Sophia, C. Zhao, C. Xu, Y. Xiang, J. Li, and H. Zhang, Black phosphorus quantum dots as an efficient saturable absorber for bound soliton operation in an erbium doped fiber laser, *IEEE Photonics J.* 8(5), 1503310 (2016)

231. J. Ma, S. Lu, Z. Guo, X. Xu, H. Zhang, D. Tang, and D. Fan, Few-layer black phosphorus based saturable absorber mirror for pulsed solid-state lasers, *Opt. Express* 23(17), 22643 (2015)

232. Y. Song, S. Chen, Q. Zhang, L. Li, L. Zhao, H. Zhang, and D. Tang, Vector soliton fiber laser passively mode locked by few layer black phosphorus-based optical saturable absorber, *Opt. Express* 24(23), 25933 (2016)

233. Y. Xu, X. F. Jiang, Y. Ge, Z. Guo, Z. Zeng, Q. H. Xu, H. Zhang, X. F. Yu, and D. Fan, Size-dependent nonlinear optical properties of black phosphorus nanosheets and their applications in ultrafast photonics, *J. Mater. Chem. C* 5(12), 3007 (2017)

234. J. Liu, J. Liu, Z. Guo, H. Zhang, W. Ma, J. Wang, and L. Su, Dual-wavelength Q-switched Er:SrF_2 laser with a black phosphorus absorber in the mid-infrared region, *Opt. Express* 24(26), 30289 (2016)

235. J. Du, M. Zhang, Z. Guo, J. Chen, X. Zhu, G. Hu, P. Peng, Z. Zheng, and H. Zhang, Phosphorene quantum dot saturable absorbers for ultrafast fiber lasers, *Sci. Rep.* 7(1), 42357 (2017)

236. Y. Wang, J. Li, L. Han, R. Lu, Y. Hu, Z. Li, and Y. Liu, Q-switched Tm^{3+}-doped fiber laser with a microfiber based black phosphorus saturable absorber, *Laser Phys.* 26(6), 065104 (2016)

237. Y. Zhang, X. Li, A. Qyyum, T. Feng, P. Guo, J. Jiang, and H. Zheng, PbS nanoparticles for ultrashort pulse generation in optical communication region, *Particle & Particle Systems Characterization* 35(11), 1800341 (2018)

238. L. Yun, Y. Qiu, C. Yang, J. Xing, K. Yu, X. Xu, and W. Wei, PbS quantum dots as a saturable absorber for ultrafast laser, *Photon. Res.* 6(11), 1028 (2018)

239. J. Liu, H. Huang, F. Zhang, Z. Zhang, J. Liu, H. Zhang, and L. Su, Bismuth nanosheets as a Q-switcher for a mid-infrared erbium-doped SrF_2 laser, *Photon. Res.* 6(8), 762 (2018)

240. M. Pumera and Z. Sofer, 2D monoelemental arsenene, antimonene, and bismuthene: Beyond black phosphorus, *Adv. Mater.* 29(21), 1605299 (2017)

241. L. Lu, W. Wang, L. Wu, X. Jiang, Y. Xiang, J. Li, D. Fan, and H. Zhang, All-optical switching of two continuous waves in few layer bismuthene based on spatial cross-phase modulation, *ACS Photon.* 4(11), 2852 (2017)

242. Q. Wang, Y. Chen, G. Jiang, L. Miao, C. Zhao, X. Fu, S. Wen, and H. Zhang, Drop-casted self-assembled topological insulator membrane as an effective saturable absorber for ultrafast laser photonics, *IEEE Photon. J.* 7(2), 1500911 (2015)

243. Q. Wang, Y. Chen, L. Miao, G. Jiang, S. Chen, J. Liu, X. Fu, C. Zhao, and H. Zhang, Wide spectral and wavelength-tunable dissipative soliton fiber laser with topological insulator nano-sheets self-assembly films sandwiched by PMMA polymer, *Opt. Express* 23(6), 7681 (2015)

244. M. Liu, N. A. Zhao, H. Liu, X.W. Zheng, A.P. Luo, Z.C. Luo, W.C. Xu, C.J. Zhao, H. Zhang, and S.C. Wen, Dual-wavelength harmonically mode-locked fiber laser with topological insulator saturable absorber, *IEEE Photon. Technol. Lett.* 26(10), 983 (2014)

245. X. Jiang, S. Liu, W. Liang, S. Luo, Z. He, Y. Ge, H. Wang, R. Cao, F. Zhang, Q. Wen, J. Li, Q. Bao, D. Fan, and H. Zhang, Broadband nonlinear photonics in few-layer MXene $Ti_3C_2T_x$ (T = F, O, or OH), *Laser Photon. Rev.* 12(2), 1700229 (2018)

246. X. Y. Feng, B. Y. Ding, W. Y. Liang, F. Zhang, T. Y. Ning, J. Liu, and H. Zhang, MXene $Ti_3C_2T_x$ absorber for a 1.06 μm passively Q-switched ceramic laser, *Laser Phys. Lett.* 15(8), 085805 (2018)

247. Y. Zu, C. Zhang, X. Guo, W. Liang, J. Liu, L. Su, and H. Zhang, A solid-state passively Q-switched Tm,Gd:CaF_2 laser with a $Ti_3C_2T_x$ MXene absorber near 2 μm, *Laser Phys. Lett.* 16(1), 015803 (2019)

248. Y. Song, Z. Liang, X. Jiang, Y. Chen, Z. Li, L. Lu, Y. Ge, K. Wang, J. Zheng, S. Lu, J. Ji, and H. Zhang, Few-layer antimonene decorated microfiber: Ultra-short pulse generation and all-optical thresholding with enhanced long term stability, *2D Mater.* 4(4), 045010 (2017)

249. P. Li, Y. Chen, T. Yang, Z. Wang, H. Lin, Y. Xu, L. Li, H. Mu, B. N. Shivananju, Y. Zhang, Q. Zhang, A. Pan, S. Li, D. Tang, B. Jia, H. Zhang, and Q. Bao, Two-dimensional $CH_3NH_3PbI_3$ perovskite nanosheets for ultrafast pulsed fiber lasers, *ACS Appl. Mater. Interfaces* 9(14), 12759 (2017)

250. Z. Sun, T. Hasan, F. Torrisi, D. Popa, G. Privitera, F. Wang, F. Bonaccorso, D. M. Basko, and A. C. Ferrari, Graphene mode-locked ultrafast laser, *ACS Nano* 4(2), 803 (2010)

251. W. Li, B. Chen, C. Meng, W. Fang, Y. Xiao, X. Li, Z. Hu, Y. Xu, L. Tong, H. Wang, W. Liu, J. Bao, and Y. R. Shen, Ultrafast all-optical graphene modulator, *Nano Lett.* 14(2), 955 (2014)

252. J. Li, H. Luo, B. Zhai, R. Lu, Z. Guo, H. Zhang, and Y. Liu, Black phosphorus: A two-dimension saturable absorption material for mid-infrared Q-switched and mode-locked fiber lasers, *Sci. Rep.* 6(1), 30361 (2016)

253. X. M. Liu, H. R. Yang, Y. D. Cui, G. W. Chen, Y. Yang, X. Q. Wu, X. K. Yao, D. D. Han, X. X. Han, C. Zeng, J. Guo, W. L. Li, G. Cheng, and L. M. Tong, Graphene-clad microfibre saturable absorber for ultrafast fibre lasers, *Sci. Rep.* 6(1), 26024 (2016)

254. S. Yu, X. Wu, Y. Wang, X. Guo, and L. Tong, 2D materials for optical modulation: Challenges and opportunities, *Adv. Mater.* 29(14), 1606128 (2017)

255. F. Wang, Y. Zhang, C. Tian, C. Girit, A. Zettl, M. Crommie, and Y. R. Shen, Gate-variable optical transitions in graphene, *Science* 320(5873), 206 (2008)

256. Z. Sun, T. Hasan, F. Torrisi, D. Popa, G. Privitera, F. Wang, F. Bonaccorso, D. M. Basko, and A. C. Ferrari, Graphene mode-locked ultrafast laser, *ACS Nano* 4(2), 803 (2010)

257. D. B. S. Soh, R. Hamerly, and H. Mabuchi, Comprehensive analysis of the optical Kerr coefficient of graphene, *Phys. Rev. A* 94, 023845 (2016)

258. E. Pop, V. Varshney, and A. K. Roy, Thermal properties of graphene: Fundamentals and applications, *MRS Bull.* 37(12), 1273 (2012)

259. Y. Wu, X. Yan, P. Meng, P. Sun, G. Cheng, and R. Zheng, Carbon black/octadecane composites for room temperature electrical and thermal regulation, *Carbon* 94, 417 (2015)

260. L. Wu, X. Jiang, J. Zhao, W. Liang, Z. Li, W. Huang, Z. Lin, Y. Wang, F. Zhang, S. Lu, Y. Xiang, S. Xu, J. Li, and H. Zhang, MXene-based nonlinear optical information converter for all-optical modulator and switcher, *Laser Photon. Rev.* 12(12), 215 (2018)

261. G. M. Paternò, L. Moretti, A. J. Barker, Q. Chen, K. Müllen, A. Narita, G. Cerullo, F. Scotognella, and G. Lanzani, Pump-push-probe for ultrafast all-optical switching: The case of a nanographene molecule, *Adv. Funct. Mater.* 29(21), 1805249 (2018)

262. J. Zheng, Z. Yang, C. Si, Z. Liang, X. Chen, R. Cao, Z. Guo, K. Wang, Y. Zhang, J. Ji, M. Zhang, D. Fan, and H. Zhang, Black phosphorus based all-optical-signal-processing: Toward high performances and enhanced stability, *ACS Photon.* 4(6), 1466 (2017)

263. S. Chen, L. Miao, X. Chen, Y. Chen, C. Zhao, S. Datta, Y. Li, Q. Bao, H. Zhang, Y. Liu, S. Wen, and D. Fan, Few-layer topological insulator for all-optical signal processing using the nonlinear Kerr effect, *Adv. Opt. Mater.* 3(12), 1769 (2015)

264. Y. Wang, F. Zhang, X. Tang, X. Chen, Y. Chen, W. Huang, Z. Liang, L. Wu, Y. Ge, Y. Song, J. Liu, D. Zhang, J. Li, and H. Zhang, All-optical phosphorene phase modulator with enhanced stability under ambient conditions, *Laser Photon. Rev.* 12(6), 1800016 (2018)

265. J. Zheng, X. Tang, Z. Yang, Z. Liang, Y. Chen, K. Wang, Y. Song, Y. Zhang, J. Ji, Y. Liu, D. Fan, and H. Zhang, Few-layer phosphorene-decorated microfiber for all-optical thresholding and optical modulation, *Adv. Opt. Mater.* 5(9), 1700026 (2017)

266. B. Sensale-Rodriguez, R. Yan, M. M. Kelly, T. Fang, K. Tahy, W. S. Hwang, D. Jena, L. Liu, and H. G. Xing, Broadband graphene terahertz modulators enabled by intraband transitions, *Nat. Commun.* 3(1), 780 (2012)

267. B. Sensale-Rodriguez, T. Fang, R. Yan, M. M. Kelly, D. Jena, L. Liu, and H. Xing, Unique prospects for graphene-based terahertz modulators, *Appl. Phys. Lett.* 99(11), 113104 (2011)

268. Q. Y. Wen, W. Tian, Q. Mao, Z. Chen, W. W. Liu, Q. H. Yang, M. Sanderson, and H. W. Zhang, Graphene based all-optical spatial terahertz modulator, *Sci. Rep.* 4(1), 7409 (2015)

269. Y. Yao, M. A. Kats, R. Shankar, Y. Song, J. Kong, M. Loncar, and F. Capasso, Wide wavelength tuning of optical antennas on graphene with nanosecond response time, *Nano Lett.* 14(1), 214 (2014)

270. N. K. Emani, T. F. Chung, X. Ni, A. V. Kildishev, Y. P. Chen, and A. Boltasseva, Electrically tunable damping of plasmonic resonances with graphene, *Nano Lett.* 12(10), 5202 (2012)

271. Z. Shi, L. Gan, T. H. Xiao, H. L. Guo, and Z. Y. Li, All-optical modulation of a graphene-cladded silicon photonic crystal cavity, *ACS Photon.* 2(11), 1513 (2015)

272. S. H. Lee, M. Choi, T. T. Kim, S. Lee, M. Liu, X. Yin, H. K. Choi, S. S. Lee, C. G. Choi, S. Y. Choi, X. Zhang, and B. Min, Switching terahertz waves with gate-controlled active graphene metamaterials, *Nat. Mater.* 11(11), 936 (2012)

273. Z. Huang, W. Han, H. Tang, L. Ren, D. S. Chander, X. Qi, and H. Zhang, Photoelectrochemical-type sunlight photodetector based on MoS_2/graphene heterostructure, *2D Mater.* 2(3), 035011 (2015).

274. X. Ren, Z. Li, Z. Huang, D. Sang, H. Qiao, X. Qi, J. Li, J. Zhong, and H. Zhang, Environmentally robust black phosphorus nanosheets in solution: Application for self-powered photodetector, *Adv. Funct. Mater.* 27(18), 1606834 (2017)

275. P. Guo, J. Xu, K. Gong, X. Shen, Y. Lu, Y. Qiu, J. Xu, Z. Zou, C. Wang, H. Yan, Y. Luo, A. Pan, H. Zhang, J. design for high-performance photodetectors, *ACS Nano* 10(9), 8474 (2016)

276. Z. Sun, Y. Zhao, Z. Li, H. Cui, Y. Zhou, W. Li, W. Tao, H. Zhang, H. Wang, P. K. Chu, and X. F. Yu, TiL_4-coordinated black phosphorus quantum dots as an efficient contrast agent for *in vivo* photoacoustic imaging of cancer, *Small* 13(11), 1602896 (2017)

277. H. Xie, Z. Li, Z. Sun, J. Shao, X. F. Yu, Z. Guo, J. Wang, Q. Xiao, H. Wang, Q. Q. Wang, H. Zhang, and P. K. Chu, Metabolizable ultrathin Bi_2Se_3 nanosheets in imaging-guided photothermal therapy, *Small* 12(30), 4136 (2016)

278. W. Tao, X. Ji, X. Xu, M. A. Islam, Z. Li, S. Chen, P. E. Saw, H. Zhang, Z. Bharwani, Z. Guo, J. Shi, and O. C. Farokhzad, Antimonene quantum dots: Synthesis and application as near-infrared photothermal agents for effective cancer therapy, *Angew. Chem. Int. Ed. Engl.* 56(39), 11896 (2017)

279. F. Yin, K. Hu, S. Chen, D. Wang, J. Zhang, M. Xie, D. Yang, M. Qiu, H. Zhang, and Z. Li, Black phosphorus quantum dot based novel siRNA delivery systems in human pluripotent teratoma PA-1 cells, *J. Mater. Chem. B* 5(27), 5433 (2017)

280. M. Qiu, D. Wang, W. Liang, L. Liu, Y. Zhang, X. Chen, D. K. Sang, C. Xing, Z. Li, B. Dong, F. Xing, D. Fan, S. Bao, H. Zhang, and Y. Cao, Novel concept of the smart NIR-light-controlled drug release of black phosphorus nanostructure for cancer therapy, *Proc. Natl. Acad. Sci. USA* 115(3), 501 (2018)

281. T. Wang, Y. Guo, P. Wan, H. Zhang, X. Chen, and X. Sun, Flexible transparent electronic gas sensors, *Small* 12(28), 3748 (2016)

282. P. Wan, X. Wen, C. Sun, B. K. Chandran, H. Zhang, X. Sun, and X. Chen, Flexible transparent films based on nanocomposite networks of polyaniline and carbon nanotubes for high-performance gas sensing, *Small* 11(40), 5409 (2015)

283. T. Wang, Y. Guo, P. Wan, X. Sun, H. Zhang, Z. Yu, and X. Chen, A flexible transparent colorimetric wrist strap sensor, *Nanoscale* 9(2), 869 (2017)

284. X. Chen, G. Xu, X. Ren, Z. Li, X. Qi, K. Huang, H. Zhang, Z. Huang, and J. Zhong, A black/red phosphorus hybrid as an electrode material for high-performance Li-ion batteries and supercapacitors, *J. Mater. Chem. A* 5(14), 6581 (2017)

285. R. Wang, X. Li, Z. Wang, and H. Zhang, Electrochemical analysis graphite/electrolyte interface in lithium-ion batteries: p-toluenesulfonyl isocyanate as electrolyte additive, *Nano Energy* 34, 131 (2017)

286. D. Mao, S. L. Zhang, Y. D. Wang, X. T. Gan, W. D. Zhang, T. Mei, Y. G. Wang, Y. S. Wang, H. B. Zeng, and J. L. Zhao, WS_2 saturable absorber for dissipative soliton mode locking at 1.06 and 1.55 m, *Opt. Express* 23(21), 27509 (2015)